The Surface Chemistry of Colloidal Lead Halide Perovskite Nanowires

Alexander M. Oddo,[1,2] Marcel Arnold,[3] and Peidong Yang[1,2,3,4,]*

1 Department of Chemistry, University of California, Berkeley, Berkeley, California 94720, United States

2 Materials Sciences Division, Lawrence Berkeley National Laboratory, Berkeley, California 94720, United States

3 Kavli Energy NanoScience Institute, Berkeley, California 94720, United States

4 Department of Materials Science and Engineering, University of California, Berkeley, Berkeley, California 94720, United States

Corresponding Author

* Peidong Yang, Email: p_yang@berkeley.edu

This study explored the interplay between the ligand-surface chemistry of colloidal $CsPbBr_3$ nanowires (NWs) and their optical properties. The ligand equilibrium was probed using nuclear magnetic resonance spectroscopy and, by perturbing the equilibrium via dilution, the gradual removal of ligands from the $CsPbBr_3$ surface was observed. This removal was correlated to an increase in the surface defect density, as suggested by a broadening of the photoluminescence (PL) spectrum, decrease in the PL quantum yield (PLQY), and quenching of the PL decay. These results highlight similar surface binding between the traditional $CsPbBr_3$ quantum dots and our NWs, thereby expanding the scope of well-established ligand chemistry to a relatively unexplored nanocrystal morphology. By controlling the dilution factor, it was revealed that $CsPbBr_3$ NWs achieve a PLQY of 72 ± 2% and an relatively long average PL lifetime of 400 ± 10 ns, without relying on additional surface passivation techniques, like ligand exchange.

TOC Graphic

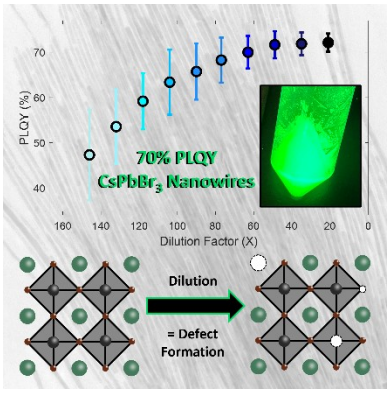

Keywords: Ligands, Nanocrystal, Perovskite, Inorganic compounds, Transmission electron microscopy

Introduction

Lead halide perovskite, represented by the formula $APbX_3$ (where A = Cs^+, MA^+, or FA^+ cations and X = Cl^-, Br^-, or I^- anions), has stood out as a cost-effective and tunable semiconducting material for light-emitting and solar energy conversion devices.[1,2] In particular, colloidal nanocrystals (NCs) of $CsPbBr_3$ have been fundamental in probing and understanding the optoelectronic properties of perovskite materials to maximize their application.[1,2] One aspect that has risen as a critical factor in determining the optoelectronic properties of colloidal $CsPbBr_3$ NCs is their surface chemistry.

Efforts to optimize the surface chemistry of colloidal $CsPbBr_3$ NCs have successfully returned quantum dots (QDs) with a photoluminescence quantum yield (PLQY) of near unity.[3-9] Surface treatment strategies, such as surface etching,[3,4] ligand exchange,[5-8] and direct synthesis with superior passivating ligands have proven robust.[9,10] These surface-targeted approaches are successful because the ionicity of the $CsPbBr_3$ lattice enables the diffusion of vacancies from the QD interior to the surface, where they function to trap radiative processes.[11] Therefore, unlike conventional metal chalcogenide semiconductors or bulk crystals, the optical performance of this ionic class of nanomaterial relies primarily on its surface chemistry.

Consequently, the need for an ideal surface ligand that effectively passivates the trap states of colloidal $CsPbBr_3$ has motivated the exploration of an ever-expanding parameter space. Colloidal $CsPbBr_3$ QDs with near-unity PLQY have been achieved by replacing the native oleic acid and

oleylamine ligands via exchange with thiourea,[3] benzoic acid,[6,7] and alkyl ammonium bromide ligands,[8] to name a few. From collected efforts, a broadly applicable set of principles has emerged that are known to generally cultivate superior optical properties among colloidal $CsPbBr_3$ QDs: 1) the removal of Cs, Pb, Br, and ligands reduces the PLQY, [12,13] 2) their PLQY can be improved by the reintroduction of ligands to underpassivated QDs,[3-8,13] 3) the same is true by the reintroduction of Cs, Pb, and Br,[14] 4) their PLQY is higher when the ligand-surface interaction is strong and the ligand-solvent interaction is weak,[13-15] and 5) surface ligand removal portends structural degradation and the loss of colloidal stabilty.[16]

It remains unclear how these principles translate to other morphologies of $CsPbBr_3$. The first colloidally synthesized $CsPbBr_3$ nanowire (NW) morphology was reported by our group in 2015 following the seminal report of $CsPbBr_3$ QDs by the Kovolenko group.[17-20] Currently, the highest reported PLQY of 10 nm-thick colloidal $CsPbBr_3$ NWs is 38%,[21] lagging behind the near-unity values achieved for typical $CsPbBr_3$ QDs.[3-10] This disparity is perplexing because near-unity PLQY should be attainable as long as the surface is completely passivated based on the aforementioned understanding of colloidal $CsPbBr_3$ surface chemistry.[3-14] Therefore, the aim of this study is to address the PLQY gap between morphologies by investigating how the established principles extend from the $CsPbBr_3$ QD model system to the $CsPbBr_3$ NW. Our ultimate goal is to stimulate greater interest in perovskite NWs as viable candidates for optoelectronic devices, especially those that may favor the use of one-dimensional semiconductors. By employing a combination of nuclear magnetic resonance (NMR) and optical spectroscopies, we uncover the underlying reasons for the initially low PLQY of as-synthesized $CsPbBr_3$ NWs and implement a method that maintains their surface condition to enhance the

optical properties to a record 72 ± 2% PLQY and ultralong 400 ± 10 ns PL lifetime without the need for ligand exchange.

Methods

Cs_2CO_3 (99.9%, Aldrich), $PbBr_2$ (99.999%, Aldrich), 1-octadecene (ODE, 90%, Aldrich), octylamine (OctAm, Aldrich, 99%), oleic acid (OA, 90%, Aldrich), oleylamine (OAm, Aldrich, 70%), molecular sieves (Sigma, 4Å), hexanes (99.9%, Fisher Scientific), deuterated toluene (d6, 99.9%, Fisher Scientific). Hexanes, d6, and OctAm were dried using molecular sieves before use. All other chemicals were used as received.

400 mg Cs_2CO_3, 15 mL ODE, and 1.4 mL OA were loaded into a 3-neck flask. This mixture was degassed and dried under vacuum with a Schlenk line and heated at 120°C while stirring at 300 rpm until the solution turned clear, typically 45 min. The resulting Cs-oleate solution was heated to 155°C for use in the synthesis of the $CsPbBr_3$ NWs and NCs. The specified temperature was that of the oil bath.

The $CsPbBr_3$ NWs were synthesized based on a previously reported method with modifications. 69 mg $PbBr_2$, 8 mL ODE, 0.5 mL OA, and 0.5 mL OAm were loaded into a 3-neck flask and degassed under vacuum with a Schlenk line while heating at 100°C for 40 min. The solution was stirred at 700 rpm throughout. Following degassing, 0.5 mL OctAm was injected at 100°C under argon flow and then the temperature was raised to 120°C. After 10 min, 0.6 mL of Cs-oleate solution at 155°C was quickly injected into the $PbBr_2$/ligand solution. After 20 min, the reaction was quenched via rapid cooling to room temperature using a water bath. The specified temperature was that of the reaction as monitored by an internal temperature probe. The reaction mixture was then purified by centrifugation at 6,000 rpm for 5 min to obtain $CsPbBr_3$ NWs.

The $CsPbBr_3$ NCs were synthesized based on a previously reported method with modifications.[18,19] 69 mg $PbBr_2$, 8 mL ODE, 0.5 mL OA, and 0.5 mL OAm were loaded into a 3-neck flask and degassed under vacuum with a Schlenk line while heating at 100°C for 40 min. The solution was stirred at 700 rpm throughout. The temperature was raised to 155°C under argon flow. Once stable, 0.4 mL of Cs-oleate solution at 155°C was quickly injected into the $PbBr_2$/ligand solution. Instantly, the reaction was quenched via rapid cooling to room temperature using an ice bath. The specified temperature was that of the reaction as monitored by an internal temperature probe. The reaction mixture was then purified by centrifugation at 6,000 rpm for 5 min to obtain $CsPbBr_3$ NCs. The dilution series experiments involving NMR, TEM, and PL spectroscopy in the main text were all performed on the same samples. The pellet was resuspended in 525 μL hexanes, which was our starting dilution factor of 21X based on the experience that 25 μL was the smallest possible volume that could dissolve the pellet.

NMR spectra of $CsPbBr_3$ NWs and NCs in 0.5 mL d6 were measured on a Bruker 700 MHz spectrometer with an inverse cryoprobe. 2D NOESY experiments were performed using a mixing time of 500 ms and a delay time of 7 s within a 26 min total collection time. MestReNova software was used for phase and baseline correction of the NMR spectra.

Colloidal samples were drop casted onto ultrathin carbon-coated Cu or Ni TEM grids for imaging. TEM images were acquired with the Hitachi H-7650 TEM at 100 kV. The low magnification images were taken on the Hitachi H-7650 microscope. HR-TEM images were acquired with the TEAM0.5 microscope at 80 kV. The TEAM 0.5 microscope was located at the National Center for Electron Microscopy. Focal series data were acquired and processed according to references 27 & 31 with minor changes. The focal series was recorded from -20 nm

to 0 nm defocus with a 2 nm step to avoid sample drift, and the beam was not monochromated. Exit wave reconstruction was carried out on the focal series in Matlab R2023a.

UV-vis absorption spectra were acquired by a Shimadzu UV-2600 spectrophotometer equipped with an integrating sphere. Steady-state PL and PLQY data were obtained under 450 nm photoexcitation using an Edinburgh FS5 spectrophotometer with a 150 W Xe-arc lamp. PL decay was measured using the Edinburgh FS5 operating in time-resolved single photon counting mode using a 375 nm pulsed diode laser, with a pulse duration of 60 ps at 10 MHz. All measurements were performed on colloidal samples suspended in hexanes in either a 1 cm or 0.1 mm cuvette. The PL lifetimes were obtained by fitting the PL decay using Fluoracle software.

The Monte Carlo simulation was conducted as prescribed in our previous work with modifications.[20] The $CsPbBr_3$ lattice was modeled in MATLAB 2023b as a three-dimensional grid of points according to the experimental lattice spacing, 2.9 Å, with a randomly distributed density of surface defects. The photoexcitation was initiated by placing an exciton at a random point on the grid at t=0. The exciton was then allowed to diffuse via random walk with a velocity based on the three-dimensional Maxwell distribution. When the exciton meets with a defect at a given lattice point, the exciton can either undergo nonradiative decay or detrapping. The detrapping probability was 0.05. If detrapping occurs, the exciton is released after a detrapping time and assigned a new velocity. With each iteration of the random walk, a new velocity is assigned to the exciton until radiative or nonradiative decay occurs. The time taken for radiative decay is based on the experimental radiative lifetime, 7 ns. To obtain the simulated PL decay spectra, 1000 photoexcitations are carried out one at a time on 10 randomly generated NWs of a certain defect density, and the observed decay time in each instance is plotted on a histogram as

the sum of the diffusion time, detrapping time, and the radiative decay time, while nonradiatively decaying excitons were excluded from the signal.

Results And Discussion

First, let us speak generally about the surface chemistry of colloidal $CsPbBr_3$ irrespective of morphology. The most established synthesis of colloidal $CsPbBr_3$ is the hot injection method, by which cesium oleate is injected into a solution containing lead bromide and long-chain carboxylic acid and amine ligands at high temperature.[17] The carboxylic acid donates a proton to the amine functionality to form a charged ligand pair capable of co-binding to the surface of $CsPbBr_3$.[1,5] This ligand pair exists in solution-state equilibrium with the individual ligands, as represented by Equation 1, where R is an organic moiety.

$$RCOOH_{(l)} + RNH_{2(l)} \rightleftharpoons RCOO^{-} \qquad (1)$$

The raw product mixture is comprised of excess ligands, complexed ligands, excess precursor, nonvolatile organic solvent (1-octadecene), and a size distribution of colloidal $CsPbBr_3$. Essentially all reports of colloidal $CsPbBr_3$ concentrate on the isolated product obtained after centrifugation.[1-20] This centrifugation step is necessary because the nonvolatile solvent and excess ligands thwart routine solid-state characterization, such as powder x-ray diffraction and transmission electron microscopy (TEM). Despite the ambiguity surrounding the true initial condition of colloidal $CsPbBr_3$ before centrifugation, acknowledging it is crucial because this unavoidable workup step is inherently a removal process that eliminates a fraction of unbound ligands from the equilibrium, as shown by Equation 2.

$$RCOOH_{(l)} + RCOO^{-} \qquad (2)$$

Following centrifugation, the obtained pellet contains $CsPbBr_3$ NCs that exhibit only partial ligand surface coverage, θ, of a given ligand, L, as dictated by the equilibrium constant, K_{eq}, in 1-octadecene.[5]

$$\theta_L = \frac{K_{eq}[L:CsPbBr_3]}{1+K_{eq}[L:CsPbBr_3]} \qquad (3)$$

The pellet is then resuspended in a volume of volatile organic solvent, typically hexanes. This introduces a new equilibrium, leading to the removal of another fraction of ligands from the $CsPbBr_3$ NCs, again dictated by Equation 3, but with the equilibrium constant in hexanes. The deterioration of the PLQY as a consequence of multiple rounds of centrifugation can be seen in Fig. S1, although we adhere to just one centrifugation cycle for the rest of this study. The $CsPbBr_3$ NCs, NWs in this case, can then be dropcasted on the TEM grid for imaging. The $CsPbBr_3$ NWs were 9 ± 1 nm-thick and 1-3 μm in length (Figure 1A & S2). Utilizing aberration-corrected high-resolution TEM (HR-TEM), the cubic unit cell was directly observed, revealing a Pb-Br bond distance of 2.9 ± 1 Å (Figure 1B).

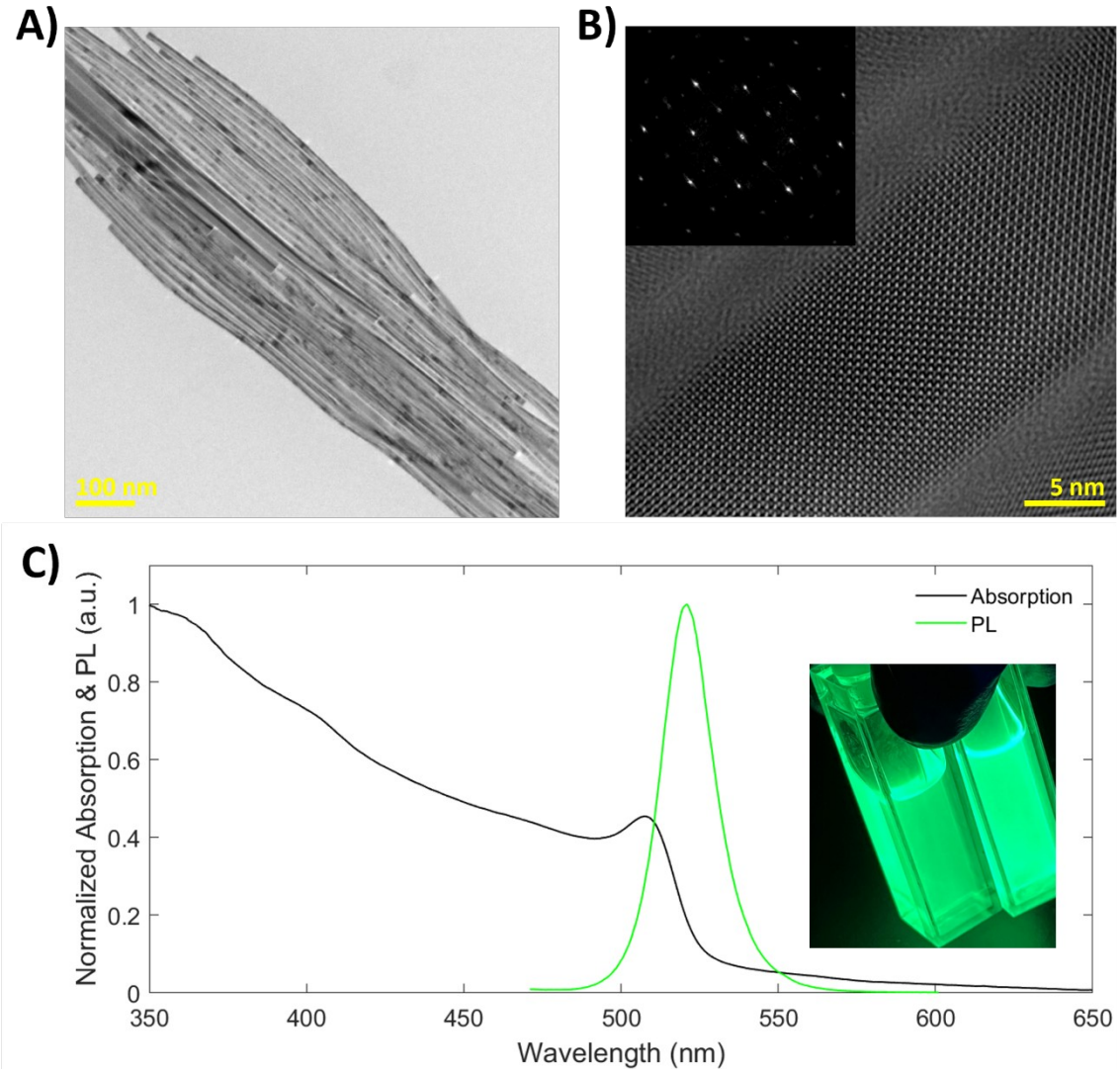

Figure 1. A) TEM image of $CsPbBr_3$ NWs**, B)** HR-TEM image of $CsPbBr_3$ NW. Inset: Fast Fourier transform (FFT) pattern of the image. **C)** Absorption and PL spectra of the $CsPbBr_3$ NWs. Inset: image of the PL of $CsPbBr_3$ NWs under 365 nm lamp photoexcitation.

For optical measurements, the $CsPbBr_3$ NWs could be further diluted in a 1 cm x 1 cm cuvette. The optical spectra of the $CsPbBr_3$ NWs contained an excitonic absorption peak around 508 nm, with the corresponding excitonic emission peak around 521 nm under 450 nm photoexcitation (Figure 1C). The standard procedure for PLQY measurements requires the preparation of

samples, such that they are optically dilute, meaning that there should be ~70% transmittance at the photoexcitation wavelength with respect to a reference solvent. This precaution aims to prevent screening and scattering effects such that the measured PLQY can be representative of the sample itself. The PLQY of $CsPbBr_3$ NWs measured under this "standard protocol" is 33%, while that of $CsPbBr_3$ QDs is 54%. The TEM characterization for 8 ± 1 nm $CsPbBr_3$ QDs is included within the Supplementary Information (Fig. S3 & S4), as it is sometimes discussed as a control system throughout this study. As previously discussed, the PLQY and ligand-surface chemistry of colloidal $CsPbBr_3$ are known to be related.[3-14]

Solution-state NMR spectroscopy is an actionable tool that has been used to investigate the surface-ligand chemistry of colloidal NCs.[22,23] In NMR spectra, the proton resonances of free ligands typically appear sharper compared to those of bound ligands proximate to the binding head.[22,23] This distinction arises from the slower diffusion of bound ligands, which exposes them to a range of environments within the timescale of the NMR measurement. Consequently, the proton resonance is broadened when it represents an average of those diverse environments. The observed proton resonance in the NMR spectrum is then a population-weighted average of free and bound ligands, or Equation 4, where λ is the experimental linewidth and N is the number of ligands.[5]

$$\lambda = \frac{N_{free}}{N_{total}} \lambda_{free} + \frac{N_{bound}}{N_{total}} \lambda_{bound} \qquad (4)$$

Therefore, narrowing of the proton resonance can be expected as the free ligand population grows and the reverse is true as the bound population grows. Indeed, the NMR spectra of the $CsPbBr_3$ NWs reveals peak narrowing for the α-carbon proton resonance of the oleylamine ligands (Figure 2A & Fig. S5), which are presumably co-bound with the carboxylic acids, as the

sample is diluted with plain organic solvent. The same is true for $CsPbBr_3$ QDs (Fig. S6). The addition of more organic solvent will disrupt the ligand-NC surface equilibrium according to the solubility of the metal-ligand complexes and ligand salts.

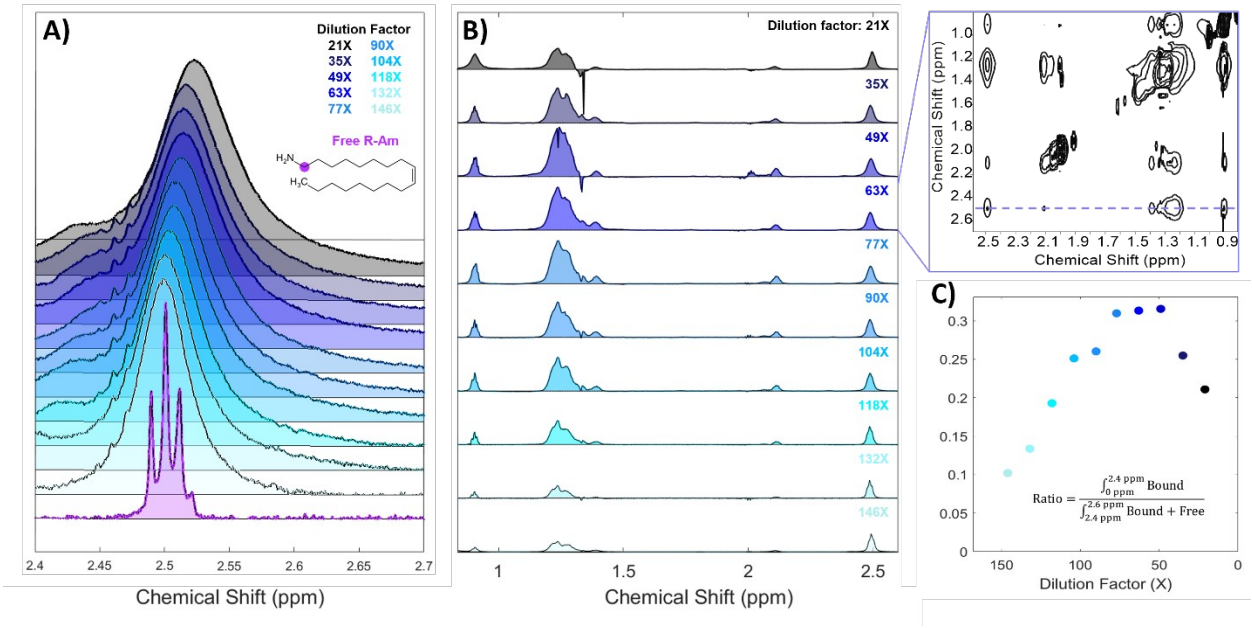

Figure 2. A) NMR spectra of $CsPbBr_3$ NWs with dilution at the oleylamine RC$\mathbf{H_2}$$NH_3$ proton resonance around 2.5 ppm. The NMR spectrum of plain oleylamine is also shown (purple). Full NMR spectra can be found at the end of the Supplementary Information. **B)** NOESY spectra of $CsPbBr_3$ NWs with dilution. Each spectrum is a horizontal slice of a 2D NOESY spectrum taken at the oleylamine RC$\mathbf{H_2}$$NH_3$ proton resonance around 2.5 ppm, as shown in the right outset. **C)** The effect of dilution on the ratio of the integral of the off-diagonal NOESY peaks across 2.5 ppm to the on-diagonal peak.

This observation of rebalancing of the bound and free ligand populations with dilution, or as more ligands are solubilized, can be seen without ambiguity using nuclear Overhauser effect spectroscopy (NOESY). NOESY is a two-dimensional (2D) NMR experiment that can differentiate bound ligands (off-diagonal peaks) from the combined signal of bound and free

ligands (on-diagonal peaks). This assignment assumes that only bound ligands generate sufficiently strong off-diagonal signals because their slow diffusion facilitates the nuclear proximity needed to promote the Overhauser effect, while freely floating ligands are too distant for cross-polarization to occur.[22,23] Indeed, the NOESY spectra of the $CsPbBr_3$ NWs (Figure 2B & 2C) at the α-carbon proton resonance of the amine ligands (along 2.5 ppm) reveals that the integrated signal of the bound ligand population compared to the on-diagonal free+bound ligand population decreases with increasing dilution. This is direct evidence that bound ligands are stripped from the $CsPbBr_3$ NW surface during the dilution process, foreshadowing the potential influence of external stimuli on optical measurements. All 2D NOESY spectra can be found in Fig. S7.

This behavior for $CsPbBr_3$ NWs aligns with the observed behavior for $CsPbBr_3$ QDs, initially reported by the Alivisatos group.[5] That is, the continued dilution of $CsPbBr_3$ with organic solvent favors the removal of Cs, Pb, and Br as charge-neutral, ligand-bound species and the formation of vacancy, V_x, because the solvent is nonpolar, as shown by Equation 5.

$$CsPbBr_3¿ \qquad (5)$$

This consistency suggests that the ligand-surface equilibrium behavior of colloidal $CsPbBr_3$ may not be entirely morphology specific. This removal process can leave behind surface vacancies that may act as trap states. This perspective also reinforces the idea that ligands with stronger ligand-surface interactions with $CsPbBr_3$ and weaker ligand-solvent interactions should aid in achieving near-unity PLQY.[3-13] However, it is crucial to emphasize that such ligands have only demonstrated their efficacy under standard measuring conditions and further dilution of even those treated $CsPbBr_3$ QDs may also eventually strip those ligands away too.

This comprehension of how seemingly innocuous external stimuli, like dilution, can impact the sensitive acid-base equilibria of colloidal $CsPbBr_3$ hints that there might be potential for improving the PLQY of NWs by adjusting standard measuring conditions. Achieving accurate PLQY measurements demands optically dilute conditions, while maintaining a less defective $CsPbBr_3$ surface necessitates minimal dilution. If the measurement of $CsPbBr_3$ NWs is carried out at the highest sample concentration possible in a 1 x 1 cm cuvette for instance, such that the entire pellet is resuspended in a volume of 2.7 mL hexanes and the transmittance is <10%, their PLQY is inadmissible because of unwanted scattering and screening effects. To reconcile both criteria, we opted for the use of a 0.1 mm pathlength cuvette. The smaller pathlength allowed for measurements to be conducted at even higher sample concentrations than normally accessible while maintaining appropriate transmission (70%), thereby avoiding defect formation induced by the ligand equilibrium under dilution and scatting/screening effects. This adjustment saw the PLQY of the $CsPbBr_3$ NWs increase to 72 ± 2%, which was higher than that of the 54% PLQY $CsPbBr_3$ QDs under standard conditions. Interestingly, the PLQY of the solution-saturated $CsPbBr_3$ QDs was near-unity, which calls into question the need for ligand exchange in that system.

The low-magnification TEM images of the 72 ± 2% PLQY $CsPbBr_3$ NWs showcase the morphological purity of the sample even at high concentration (Fig. S8). This high purity is noteworthy because the $CsPbBr_3$ QDs, being highly emissive with near-unity PLQY at this concentration, could have potentially inflated the PLQY of the NWs. Nevertheless, we confirm that the 72 ± 2% PLQY corresponds solely to the $CsPbBr_3$ NW. As for the $CsPbBr_3$ NWs and QDs measured under standard protocol in a 1 cm x 1 cm cuvette, some structural degradation was observed in the TEM images of the sample dropcasted from the cuvette (Fig. S9 & S10),

which aligns with a previous dilution study on $CsPbBr_3$ QDs.[24] This observation underscores the notion that the passivating ligand can be like a "double-edged sword," sometimes helping to improve the optical properties of perovskite NCs, but also imparting vulnerability to external stimuli. It is alarming that many relationships and fundamental phenomena concerning these NCs have been investigated without regard for dilution effects and it will be critical to design experiments in such a way to decouple the potential interference of ligand dynamics going forward, as the initial reports of $CsPbBr_3$ NWs with <40% PLQY may have underestimated their optoelectronic properties based on the interfering effect of dilution.[18-21] TEM images of the $CsPbBr_3$ NWs taken at different points throughout their dilution shows that the NW morphology is initially pristine at high concentration and then slight structural degradation becomes perceptible following dilution by a factor 146 (Fig. S11 & S12), at which point the PLQY is around 45%. Therefore, we intentionally halt our dilution series experiments at the dilution factor of 146 to focus our conclusions on the ligand chemistry without complication by any structural degradation/impurity formation.

The PLQY decrease due to the formation of vacancies on the surface of the $CsPbBr_3$ NWs (Figure 3A) and QDs (Fig. S13) could even be monitored continuously with dilution. Fig. S14 further illustrates the discrepancy in the PLQY vs. dilution trend between the use of different pathlength cuvettes, as scattering depresses the PLQY because of low transmittance (<10%) in the 1 x 1 cm cuvette while high PLQY is only accessible at higher transmittances and concentrations in the 0.1 mm pathlength cuvette, emphasizing the importance of factoring the surface chemistry of $CsPbBr_3$ NCs into experiment design.

The PL efficiency of the $CsPbBr_3$ NWs, which is related to the absolute PLQY as a function of wavelength, has been used to map the energetic footprint of the trap states in colloidal $CsPBBr_3$

nanostructures.[25] The PL efficiency spectrum, $PL_{eff}(\lambda)$, where λ is wavelength, can be calculated using equation 6.[25] A decrease in the PL efficiency with dilution is observed, which is direct evidence that the photoexcited carriers in the 390-500 nm (2.45-3.18 eV) range are quenched progressively due to the emergence of trap states in that range (Figure 3B).

$$PL_{eff}(\lambda) = \frac{Excitation\ Spectrum(\lambda)}{1 - 10^{-Absorption\ Spectrum}} \qquad (6)$$

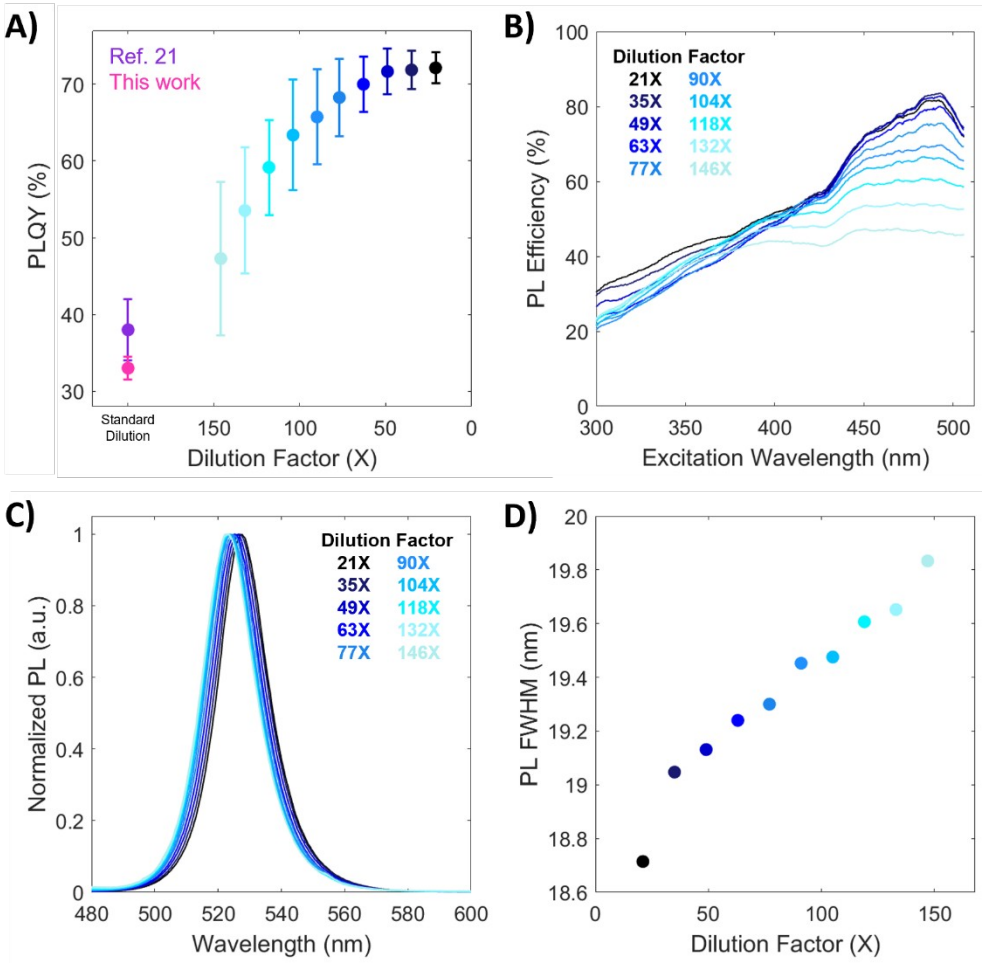

Figure 3. The effect of dilution on **A)** the PLQY, **B)** the PL efficiency, **C)** the PL spectrum, and **D)** the PL FWHM of $CsPbBr_3$ NWs.

Concurrently, the full-width half maximum (FWHM) of the exciton emission in the PL spectra increased with dilution (Figure 3C & 3D). This PL broadening, when observed at constant temperature, is a consequence of increasing defect density.[26] The PL maximum shifted from 528 nm to 523 nm with dilution. While anti-Stokes shifting of the PL can be caused by an increase in quantum confinement due to decreasing thickness,[27,28] the thickness of these $CsPbBr_3$ NWs remained unaffected by dilution. An alternative explanation could be solution-state aggregation at higher sample concentrations; for instance, a Stokes shift of 60 meV, or 12 nm, was reported for 7.9 nm $CsPbBr_3$ QDs when in an aggregated state.[29]

Finally, the triexponential PL decay of the 72 ± 2% PLQY $CsPbBr_3$ NWs was quenched upon dilution (Figure 4A). The PL lifetimes were quenched from τ_1=7.2 ns, τ_2=62.6 ns, τ_3=566 ns, and τ_{ave}=399 ns to 5.9 ns, 40.0 ns, 254 ns, and 128 ns, respectively (Figure 4B). This observation aligns with the implications of increased defect density suggested by the PLQY decrease and PL peak broadening data. These PL lifetimes are notably long-lived compared to those of 54 ± 4% $CsPbBr_3$ QDs: τ_1=2.3 ns (18.4%), τ_2=9.9 ns (78.1%), τ_3=52.9 ns (3.5%, Fig. S15), and the longest τ_3 component contributes more to the PL decay of the NWs. The PL lifetime fitting parameters can be found in Table S1. The current hypothesis for longer PL lifetimes in $CsPbBr_3$ NWs is that the τ_3 component is dominated by extended exciton diffusion along the length of the wire in addition to the exciton trapping/detrapping process,[20] whereas the τ_3 component in $CsPbBr_3$ QDs is mainly attributed to the trapping/detrapping process.[30] The relative contribution of τ_3 to the PL decay of $CsPbBr_3$ NWs decreases with dilution (Figure 4C), which suggests that the average exciton must diffuse for a shorter distance to the nearest defect before recombination takes place. This is further demonstrated using simulations: a 8 nm x 8 nm x 1 μm model NW is built with a given defect density and a kinetic Monte Carlo simulation returns quenched PL decay with

increasing defect density (Figure 4D). Therefore, the combination of PLQY, steady-state PL, and time-resolved PL data supports the conclusion that routine disruption of the ligand-surface equilibrium of colloidal $CsPbBr_3$ NWs, as corroborated by the NMR data, is the most significant factor compromising their optical properties. Furthermore, by minimizing the defect density, not only have we achieved the highest reported PLQY for $CsPbBr_3$ NWs of this size, but we have also unearthed the result that the PL decay of this system, previously reported with significant quenching,[18-20] actually extends into the microsecond range, which is longer than any reported morphology of $CsPbBr_3$, to our knowledge.

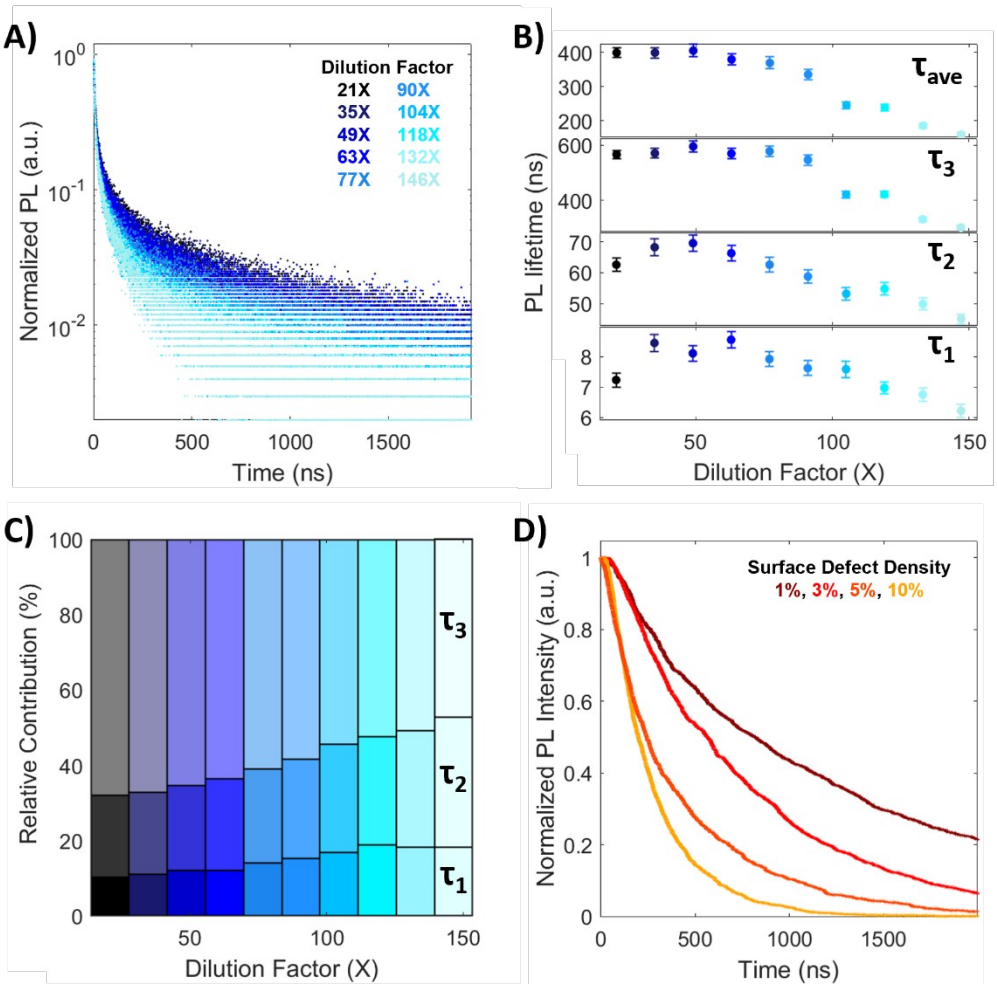

Figure 4. The effect of dilution on the **A)** PL decay, **B)** PL lifetimes, and **C)** PL lifetime relative contribution of $CsPbBr_3$ NWs. **D)** PL decay quenching results from a kinetic Monte Carlo simulation as a function of defect density.

Conclusion

In conclusion, this work delves into the interplay between the native ligand chemistry of colloidal $CsPbBr_3$ nanostructures and the resulting impact on their optical properties. The ligands for colloidal $CsPbBr_3$, widely thought of as a passivating agent for trap states, are reframed within this study as a double-edged sword that can lead to dilution-induced surface vacancy creation. This effect is a consequence of the ligand-surface equilibrium, as probed by NMR, inherent to the solution phase dynamics of this class of colloidal perovskite. We elucidated that this disruption of the ligand-surface equilibrium is the foremost challenge associated with achieving high PLQY values and long-lived photoexcited carriers in colloidal $CsPbBr_3$. High and near-unity PLQY values were achieved in $CsPbBr_3$ NWs and QDs, respectively, without the need for ligand exchange by designing an updated measurement protocol to avoid provoking this equilibrium. This study also demonstrates that the surface chemistry of $CsPbBr_3$ NWs is, in principle, similar to that of $CsPbBr_3$ QDs, although they remain unique in their optical properties, such as PLQY and long PL lifetime due to the inherent exciton diffusion behavior. This study not only enhances our understanding of the unique challenges associated with the $CsPbBr_3$ NWs, a relatively unexplored nanostructure morphology, but also offers valuable insights for future endeavors aiming to harness their full potential in optoelectronic applications.

Acknowledgements

The authors thank the staff at the NCEM; C. Song for their efforts in training the author on the TEAM 0.5 electron microscope and C. Ophus for providing the code for exit wave reconstruction. We thank Drs. Hasan Celik, Raynald Giovine, and Pines Magnetic Resonance Center's Core NMR Facility (PMRC Core) for spectroscopic assistance. The instruments used in this work were supported by the PMRC Core. This work was supported by the U.S. Department of Energy, Office of Science, Office of Basic Energy Sciences, Materials Sciences and Engineering Division, under Contract No. DE-AC02–05-CH11231 within the Fundamentals of Semiconductor Nanowire Program (KCPY23). Work at the Molecular Foundry was supported by the Office of Science, Office of Basic Energy Sciences, of the U.S. Department of Energy under Contract No. DE-AC02-05CH11231.

Author Declarations

Conflict of Interest

The authors declare no competing interests.

Author Contributions

A.M.O., M.A., and P. Y. conceived the idea and designed the research. A.M.O. and M.A. did the experiments and contributed equally. P.Y. supervised the work. All authors contributed to writing the manuscript.

Data Availability

The data that support this study are available from the corresponding author upon reasonable request.

References

1. A. Dey, J. Ye, A. De, E. Debroye, S.K. Ha, E. Bladt, A.S. Kshirsagar, Z. Wang, J. Yin, Y. Wang, L.N. Quan, F. Yan, M. Gao, X. Li, J. Shamsi, T. Debnath, M. Cao, M.A. Scheel, S. Kumar, J.A. Steele, M. Gerhard, L. Chouhan, K. Xu, X. Wu, Y. Li, Y. Zhang, A. Dutta, C. Han, I. Vincon, A.L. Rogach, A. Nag, A. Samanta, B.A. Korgel, C.-J. Shih, D.R. Gamelin, D.H. Son, H. Zeng, H. Zhong, H. Sun, H.V. Demir, I.G. Scheblykin, I. Mora-Seró, J.K. Stolarczyk, J.Z. Zhang, J. Feldmann, J. Hofkens, J.M. Luther, J. Pérez-Prieto, L. Li, L. Manna, M.I. Bodnarchuk, M. V Kovalenko, M.B.J. Roeffaers, N. Pradhan, O.F. Mohammed, O.M. Bakr, P. Yang, P. Müller-Buschbaum, P. V Kamat, Q. Bao, Q. Zhang, R. Krahne, R.E. Galian, S.D. Stranks, S. Bals, V. Biju, W.A. Tisdale, Y. Yan, R.L.Z. Hoye, and L. Polavarapu, "State of the Art and Prospects for Halide Perovskite Nanocrystals," ACS Nano **15**(7), 10775–10981 (2021).

2. J.Y. Kim, J.-W. Lee, H.S. Jung, H. Shin, and N.-G. Park, "High-Efficiency Perovskite Solar Cells," Chem. Rev. **120**(15), 7867–7918 (2020).

3. B.A. Koscher, J.K. Swabeck, N.D. Bronstein, and A.P. Alivisatos, "Essentially Trap-Free CsPbBr3 Colloidal Nanocrystals by Postsynthetic Thiocyanate Surface Treatment," J. Am. Chem. Soc. **139**(19), 6566–6569 (2017).

4. B.J. Roman, N.M. Villegas, K. Lytle, and M. Sheldon, "Optically Cooling Cesium Lead Tribromide Nanocrystals," Nano Lett. **20**(12), 8874–8879 (2020).

5. D.P. Nenon, K. Pressler, J. Kang, B.A. Koscher, J.H. Olshansky, W.T. Osowiecki, M.A. Koc, L.-W. Wang, and A.P. Alivisatos, "Design Principles for Trap-Free CsPbX3 Nanocrystals: Enumerating and Eliminating Surface Halide Vacancies with Softer Lewis Bases," J. Am. Chem. Soc. **140**(50), 17760–17772 (2018).

6. V.G.V. Dutt, S. Akhil, R. Singh, M. Palabathuni, and N. Mishra, "Year-Long Stability and Near-Unity Photoluminescence Quantum Yield of CsPbBr3 Perovskite Nanocrystals by Benzoic Acid Post-treatment," J. Phys. Chem. C **126**(22), 9502–9508 (2022).

7. Malinoski, A.; Hu, G.; Wang, C. Strong Bidentate Coordination for Surface Passivation and Ligand-Shell Engineering of Lead Halide Perovskite Nanocrystals in the Strongly Quantum-Confined Regime. *J. Phys. Chem. C* 2021, *125*, 24521–24530.

8. A. Malinoski, G. Hu, and C. Wang, "Strong Bidentate Coordination for Surface Passivation and Ligand-Shell Engineering of Lead Halide Perovskite Nanocrystals in the Strongly Quantum-Confined Regime," J. Phys. Chem. C **125**(44), 24521–24530 (2021).

9. B. Zhang, L. Goldoni, J. Zito, Z. Dang, G. Almeida, F. Zaccaria, J. de Wit, I. Infante, L. De Trizio, and L. Manna, "Alkyl Phosphonic Acids Deliver CsPbBr3 Nanocrystals with High Photoluminescence Quantum Yield and Truncated Octahedron Shape," Chem. Mater. **31**(21), 9140–9147 (2019).

10. B. Zhang, L. Goldoni, C. Lambruschini, L. Moni, M. Imran, A. Pianetti, V. Pinchetti, S. Brovelli, L. De Trizio, and L. Manna, "Stable and Size Tunable CsPbBr3 Nanocrystals Synthesized with Oleylphosphonic Acid," Nano Lett. **20**(12), 8847–8853 (2020).

11. S. ten Brinck, F. Zaccaria, and I. Infante, “Defects in Lead Halide Perovskite Nanocrystals: Analogies and (Many) Differences with the Bulk,” ACS Energy Lett. **4**(11), 2739–2747 (2019).

12. Y. Tan, Y. Zou, L. Wu, Q. Huang, D. Yang, M. Chen, M. Ban, C. Wu, T. Wu, S. Bai, T. Song, Q. Zhang, and B. Sun, “Highly Luminescent and Stable Perovskite Nanocrystals with Octylphosphonic Acid as a Ligand for Efficient Light-Emitting Diodes,” ACS Appl. Mater. Interfaces **10**(4), 3784–3792 (2018).

13. L. De Trizio, I. Infante, and L. Manna, “Surface Chemistry of Lead Halide Perovskite Colloidal Nanocrystals,” Acc. Chem. Res. **56**(13), 1815–1825 (2023).

14. S.N. Raja, Y. Bekenstein, M.A. Koc, S. Fischer, D. Zhang, L. Lin, R.O. Ritchie, P. Yang, and A.P. Alivisatos, “Encapsulation of Perovskite Nanocrystals into Macroscale Polymer Matrices: Enhanced Stability and Polarization,” ACS Appl. Mater. Interfaces **8**(51), 35523–35533 (2016).

15. J. Zito, and I. Infante, “The Future of Ligand Engineering in Colloidal Semiconductor Nanocrystals,” Acc. Chem. Res. **54**(7), 1555–1564 (2021).

16. Z. Liu, Y. Bekenstein, X. Ye, S.C. Nguyen, J. Swabeck, D. Zhang, S.-T. Lee, P. Yang, W. Ma, and A.P. Alivisatos, “Ligand Mediated Transformation of Cesium Lead Bromide Perovskite Nanocrystals to Lead Depleted Cs4PbBr6 Nanocrystals,” J. Am. Chem. Soc. **139**(15), 5309–5312 (2017).

17. L. Protesescu, S. Yakunin, M.I. Bodnarchuk, F. Krieg, R. Caputo, C.H. Hendon, R.X. Yang, A. Walsh, and M. V Kovalenko, "Nanocrystals of Cesium Lead Halide Perovskites (CsPbX3, X = Cl, Br, and I): Novel Optoelectronic Materials Showing Bright Emission with Wide Color Gamut," Nano Lett. **15**(6), 3692–3696 (2015).

18. D. Zhang, Y. Yang, Y. Bekenstein, Y. Yu, N.A. Gibson, A.B. Wong, S.W. Eaton, N. Kornienko, Q. Kong, M. Lai, A.P. Alivisatos, S.R. Leone, and P. Yang, "Synthesis of Composition Tunable and Highly Luminescent Cesium Lead Halide Nanowires through Anion-Exchange Reactions," J. Am. Chem. Soc. **138**(23), 7236–7239 (2016).

19. D. Zhang, S.W. Eaton, Y. Yu, L. Dou, and P. Yang, "Solution-Phase Synthesis of Cesium Lead Halide Perovskite Nanowires," J. Am. Chem. Soc. **137**(29), 9230–9233 (2015).

20. M. Gao, H. Liu, S. Yu, S. Louisia, Y. Zhang, D.P. Nenon, A.P. Alivisatos, and P. Yang, "Scaling Laws of Exciton Recombination Kinetics in Low Dimensional Halide Perovskite Nanostructures," J. Am. Chem. Soc. **142**(19), 8871–8879 (2020).

21. M. Imran, F. Di Stasio, Z. Dang, C. Canale, A.H. Khan, J. Shamsi, R. Brescia, M. Prato, and L. Manna, "Colloidal Synthesis of Strongly Fluorescent CsPbBr3 Nanowires with Width Tunable down to the Quantum Confinement Regime," Chem. Mater. **28**(18), 6450–6454 (2016).

22. Z. Hens, and J.C. Martins, "A Solution NMR Toolbox for Characterizing the Surface Chemistry of Colloidal Nanocrystals," Chem. Mater. **25**(8), 1211–1221 (2013).

23. J.S. Owen, J. Park, P.-E. Trudeau, and A.P. Alivisatos, "Reaction Chemistry and Ligand Exchange at Cadmium–Selenide Nanocrystal Surfaces," J. Am. Chem. Soc. **130**(37), 12279–12281 (2008).

24. Y. Tong, F. Ehrat, W. Vanderlinden, C. Cardenas-Daw, J.K. Stolarczyk, L. Polavarapu, and A.S. Urban, "Dilution-Induced Formation of Hybrid Perovskite Nanoplatelets," ACS Nano **10**(12), 10936–10944 (2016).

25. M. Liao, B. Shan, and M. Li, "Role of Trap States in Excitation Wavelength-Dependent Photoluminescence of Strongly Quantum-Confined All-Inorganic CsPbBr3 Perovskites with Varying Dimensionalities," J. Phys. Chem. C **125**(38), 21062–21069 (2021).

26. M. Gramlich, C. Lampe, J. Drewniok, and A.S. Urban, "How Exciton–Phonon Coupling Impacts Photoluminescence in Halide Perovskite Nanoplatelets," J. Phys. Chem. Lett. **12**(46), 11371–11377 (2021).

27. A.M. Oddo, M. Gao, D. Weinberg, J. Jin, M.C. Folgueras, C. Song, C. Ophus, T. Mani, E. Rabani, and P. Yang, "Energy Funneling in a Noninteger Two-Dimensional Perovskite," Nano Lett. **23**(24), 11469–11476 (2023).

28. D. Zhang, Y. Yu, Y. Bekenstein, A.B. Wong, A.P. Alivisatos, and P. Yang, "Ultrathin Colloidal Cesium Lead Halide Perovskite Nanowires," J. Am. Chem. Soc. **138**(40), 13155–13158 (2016).

29. J. Lin, L. Gomez, C. de Weerd, Y. Fujiwara, T. Gregorkiewicz, and K. Suenaga, "Direct Observation of Band Structure Modifications in Nanocrystals of CsPbBr3 Perovskite," Nano Lett. **16**(11), 7198–7202 (2016).

30. A. Dey, P. Rathod, and D. Kabra, "Role of Localized States in Photoluminescence Dynamics of High Optical Gain CsPbBr3 Nanocrystals," Adv. Opt. Mater. **6**(11), 1800109 (2018).

31. Y. Yu, D. Zhang, C. Kisielowski, L. Dou, N. Kornienko, Y. Bekenstein, A.B. Wong, A.P. Alivisatos, and P. Yang, "Atomic Resolution Imaging of Halide Perovskites," Nano Lett. **16**(12), 7530–7535 (2016).

Supporting Information for:

The Surface Chemistry of Colloidal Lead Halide Perovskite Nanowires

Alexander M. Oddo,[1,2,†] Marcel Arnold,[3,†] Peidong Yang[1,2,3,4,*]

1 Department of Chemistry, University of California, Berkeley, Berkeley, California 94720, United States

2 Materials Sciences Division, Lawrence Berkeley National Laboratory, Berkeley, California 94720, United States

3 Kavli Energy NanoScience Institute, Berkeley, California 94720, United States

4 Department of Materials Science and Engineering, University of California, Berkeley, Berkeley, California 94720, United States

* Corresponding author. E-mail: p_yang@berkeley.edu (P.Y.)

† These authors contributed equally.

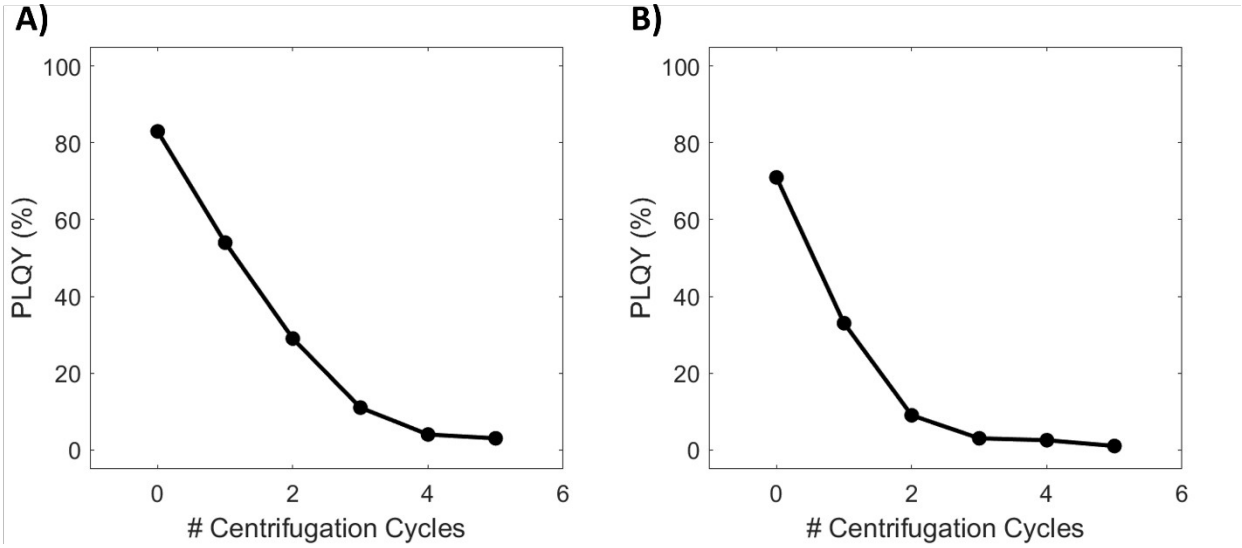

Figure S1 | Effect of centrifugation on the PLQY of $CsPbBr_3$ Nanocrystals. The dependence of the PLQY on the number of centrifugation cycles is shown for **A)** $CsPbBr_3$ QDs and **B)** $CsPbBr_3$ NWs. For demonstration purposes, the PLQY values were measured according to the standard protocol for measuring colloidal $CsPbBr_3$ NCs, optically diluted in a 1 cm x 1 cm cuvette using hexanes. Zero centrifugation cycles corresponds to measurement of the raw product.

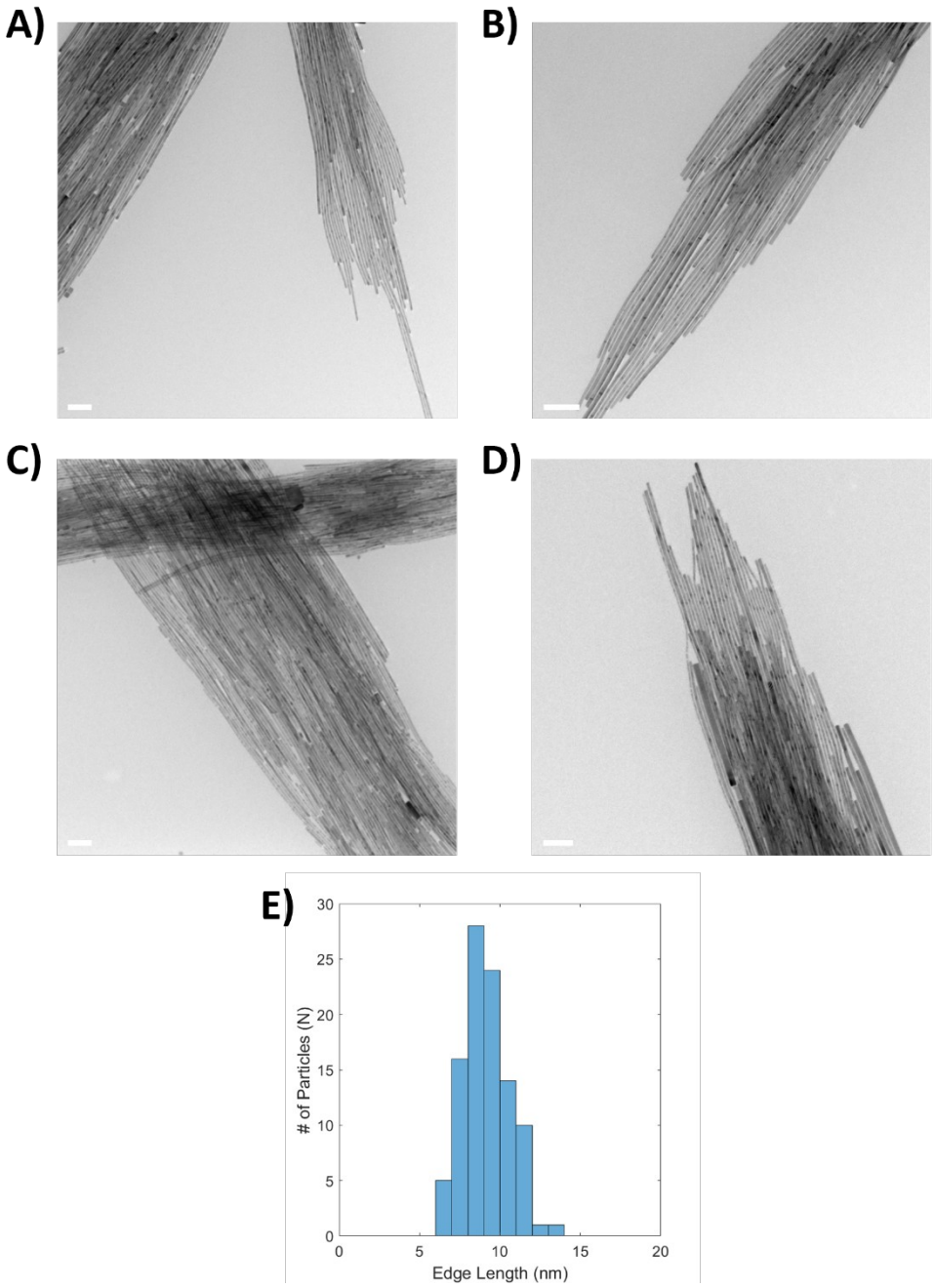

Figure S2 | Size distribution of $CsPbBr_3$ NWs. **A-D)** TEM images of $CsPbBr_3$ NWs. Scale bar: 100 nm. The sample was prepared by resuspending the $CsPbBr_3$ pellet following centrifugation in 3 mL hexanes and then dropcasting onto a TEM grid. **E)** Histogram showing the size distribution of the $CsPbBr_3$ NWs. The size of the NWs was 9 ± 1 nm based on a sample size of N=100 number of particles measured.

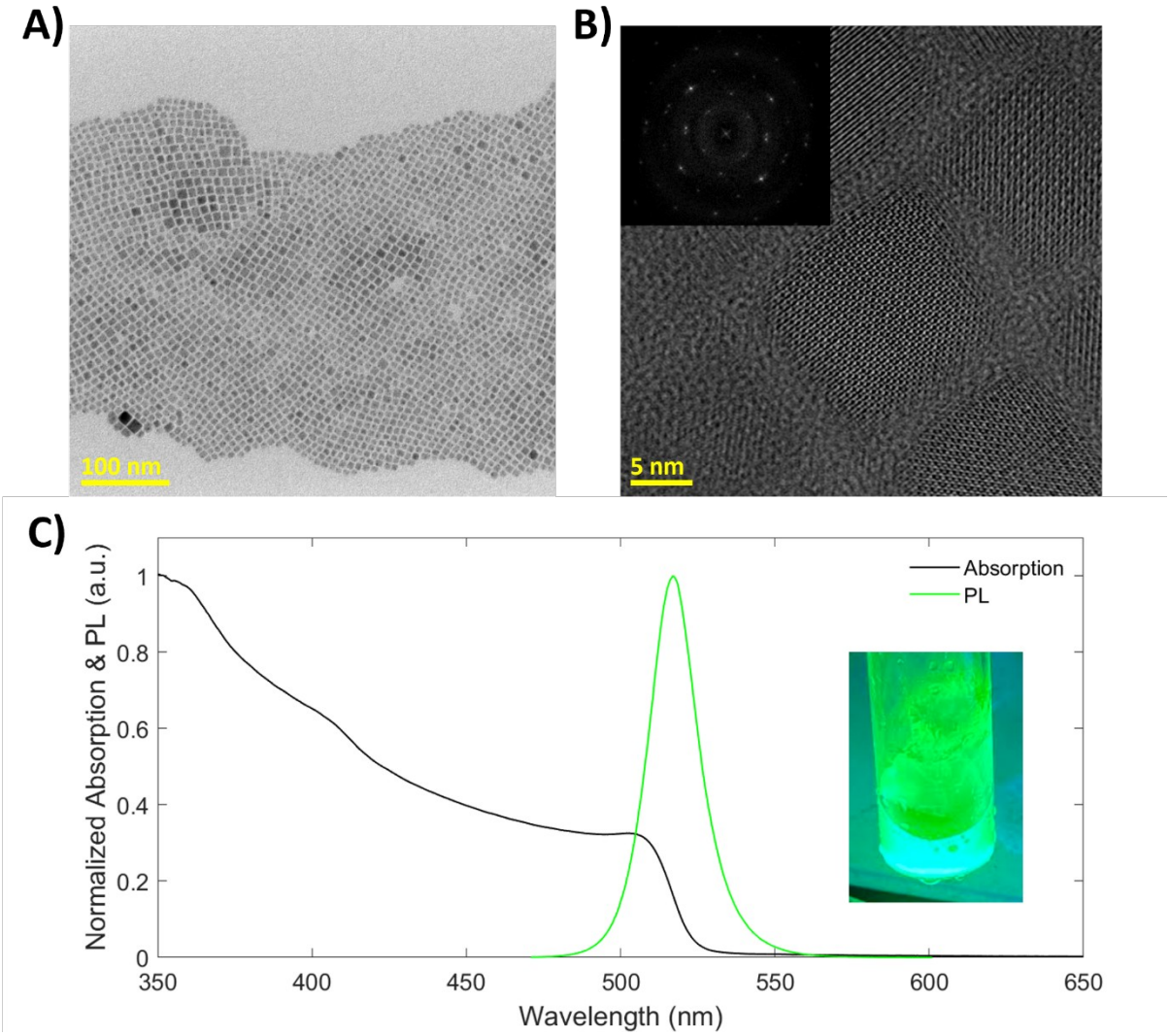

Figure S3 | Characterization of $CsPbBr_3$ QD. **A)** TEM image of $CsPbBr_3$ QDs. **B)** HR-TEM image of $CsPbBr_3$ QDs. Inset: fast Fourier transform pattern. The Pb-Br bond length was 2.9 ± 1 Å. **C)** Absorption and PL spectra of $CsPbBr_3$ QDs. Inset: image of $CsPbBr_3$ QD PL under 365 nm lamp photoexcitation.

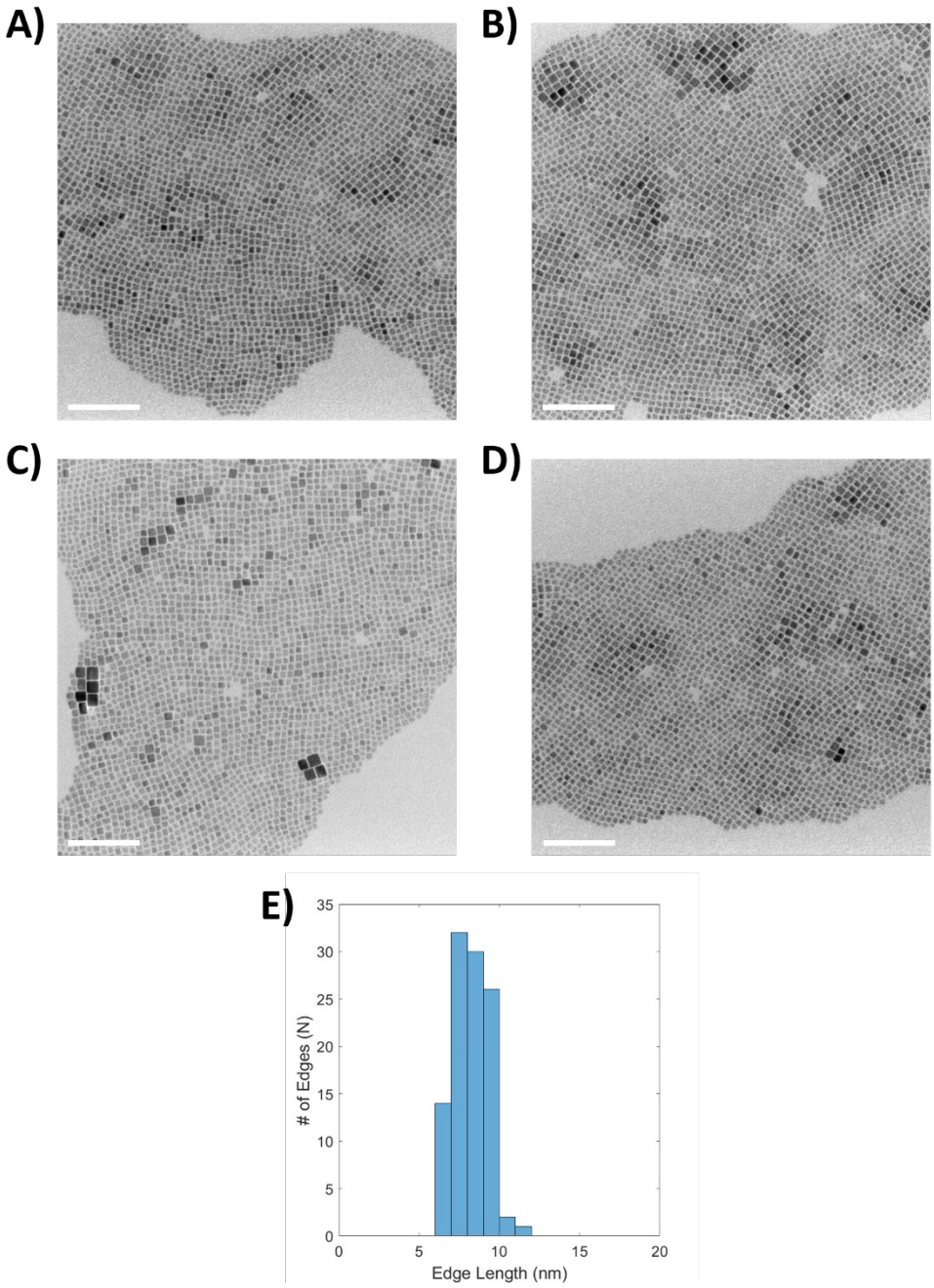

Figure S4 | Size distribution of $CsPbBr_3$ quantum dots. **A-D)** TEM images of $CsPbBr_3$ QDs. Scale bar: 100 nm. The sample was prepared by resuspending the $CsPbBr_3$ pellet following centrifugation in 3 mL hexanes and then dropcasting onto a TEM grid. **E)** Histogram showing the size distribution of the $CsPbBr_3$ QDs. The size of the QDs was 8 ± 1 nm based on a sample size of N=100 number of particles measured.

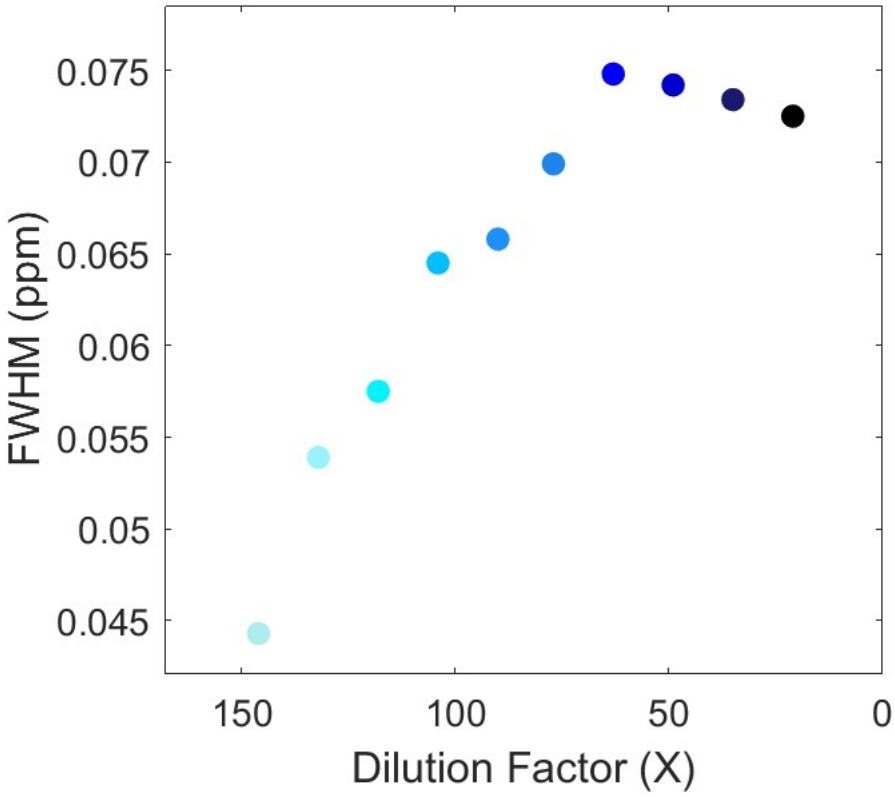

Figure S5 | Effect of dilution on the NMR linewidth of $CsPbBr_3$ NWs. The plotted full width half maxima (FWHM) correspond to fitting of the $RC\mathbf{H_2}NH_3$ resonance of the NMR spectra shown in Figure 2A of main text.

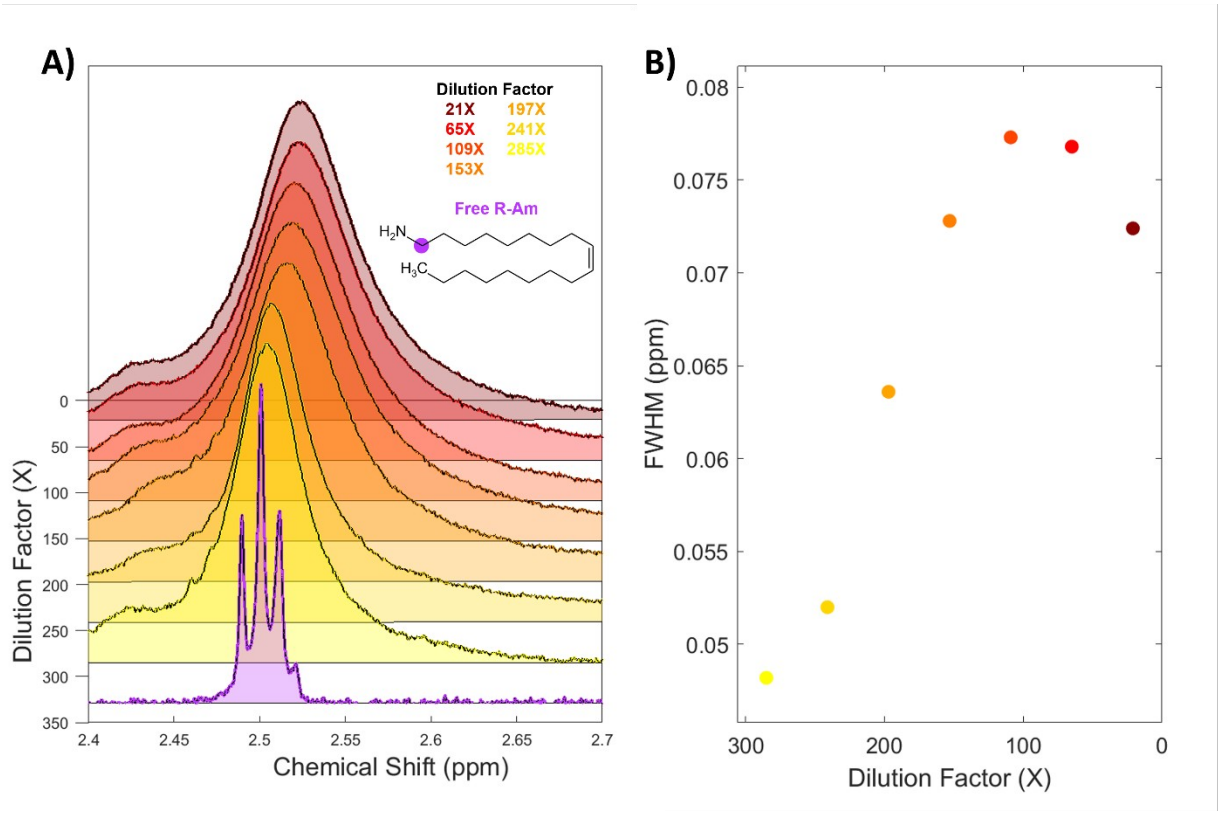

Figure S6 | A) NMR spectra of $CsPbBr_3$ QDs with dilution at the oleylamine $RC\mathbf{H_2}NH_3$ proton resonance around 2.5 ppm. The NMR spectrum of plain oleylamine is also shown (purple). Full NMR spectra can be found at the end of the Supporting Information. **B)** Effect of dilution on the NMR linewidth of $CsPbBr_3$ QDs.

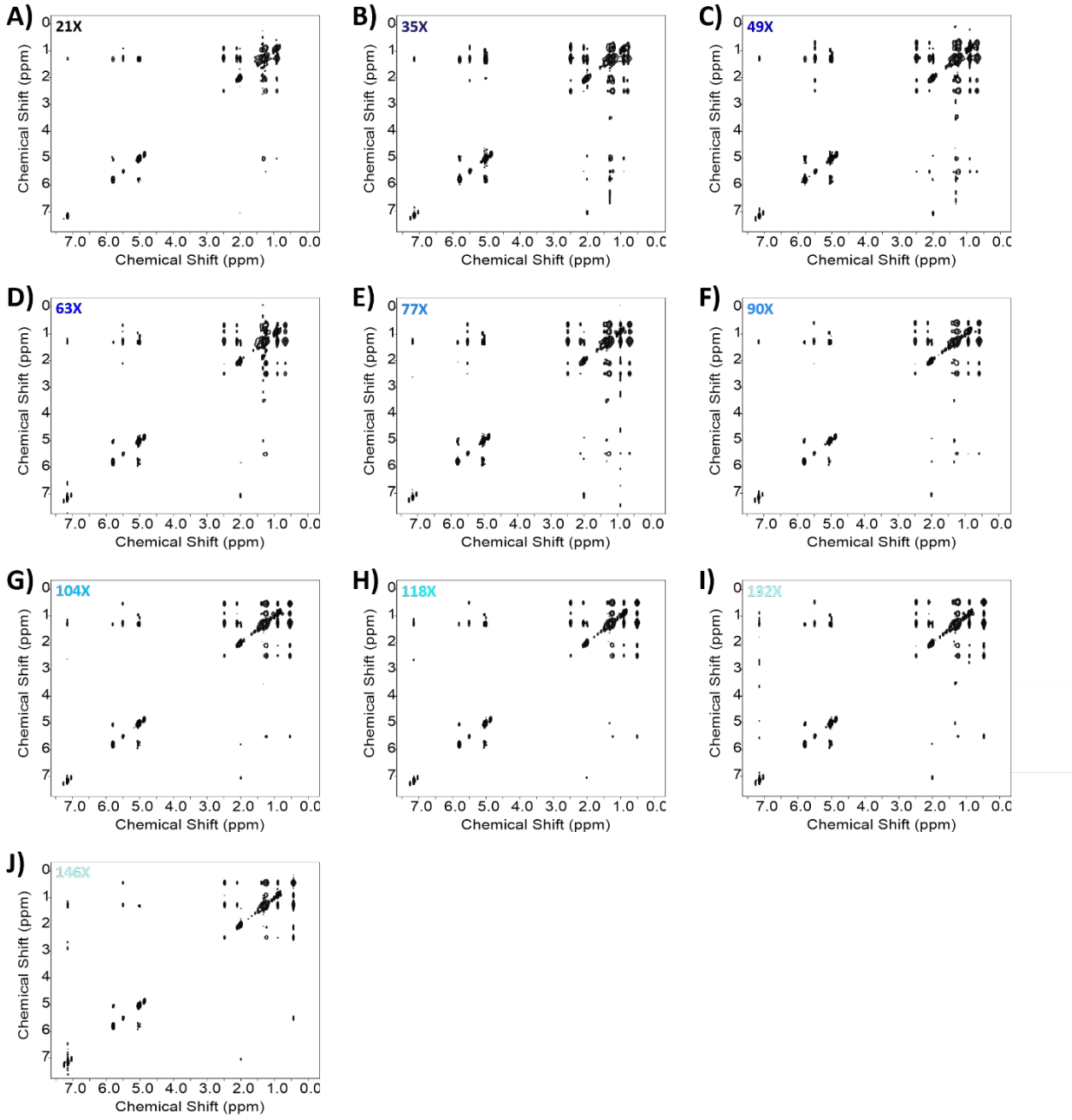

Figure S7 | Collection of 2D NOESY NMR spectra for $CsPbBr_3$ NWs as a function of dilution.

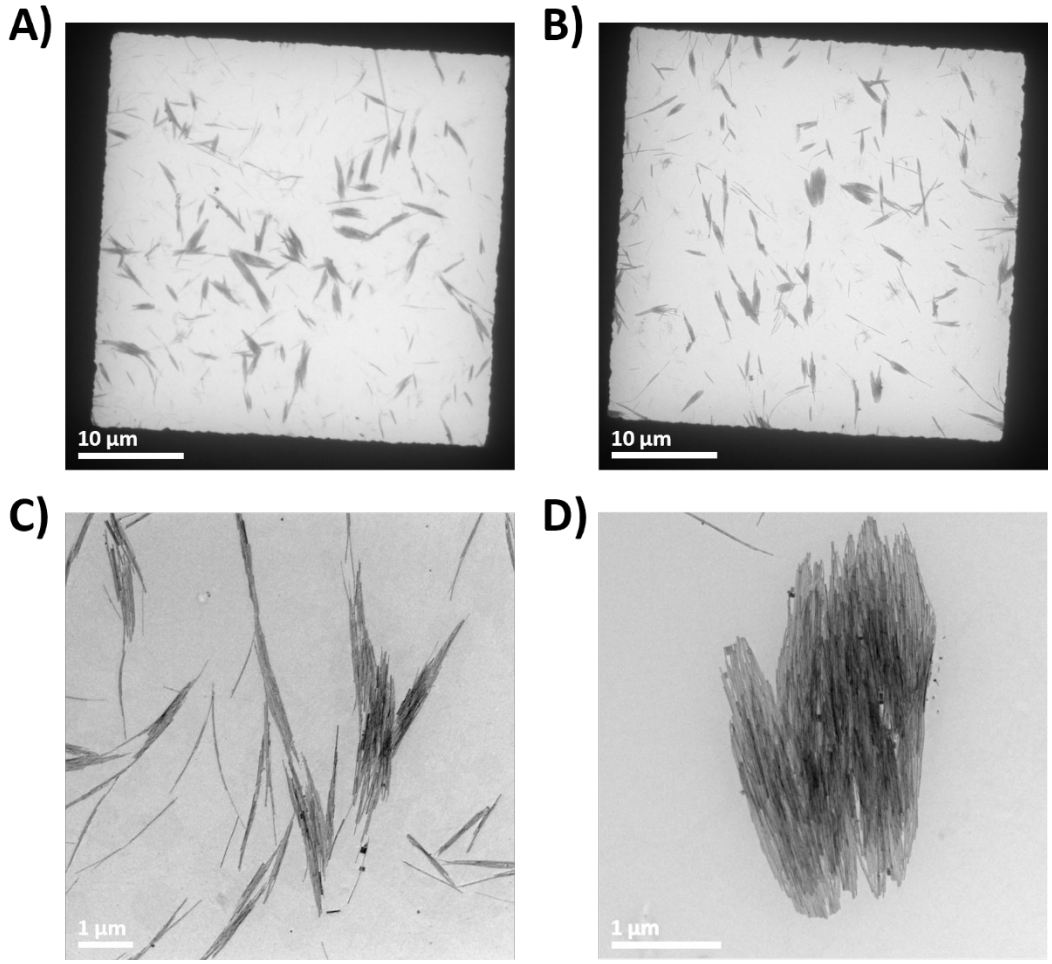

Figure S8 | Low-magnification TEM images of $CsPbBr_3$ NWs at high concentration.

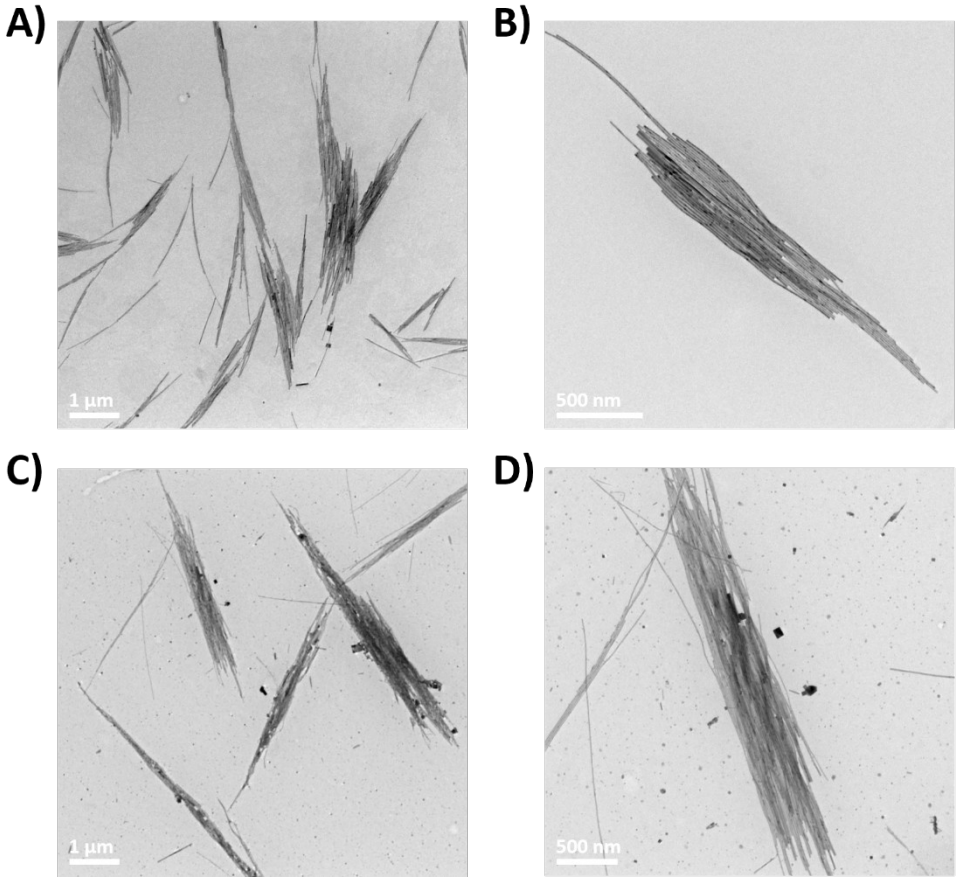

Figure S9 | Comparison of $CsPbBr_3$ NWs following dilution. TEM images of $CsPbBr_3$ QDs measured when, **A,B)** the sample is saturated in solution (21X dilution factor) and **C,D)** the sample is optically dilute in a 1 cm x 1 cm cuvette as per the standard protocol. The saturated sample was obtained by introducing a sufficiently small volume of hexanes to the pellet following centrifugation, such that the pellet cannot be fully resuspended.

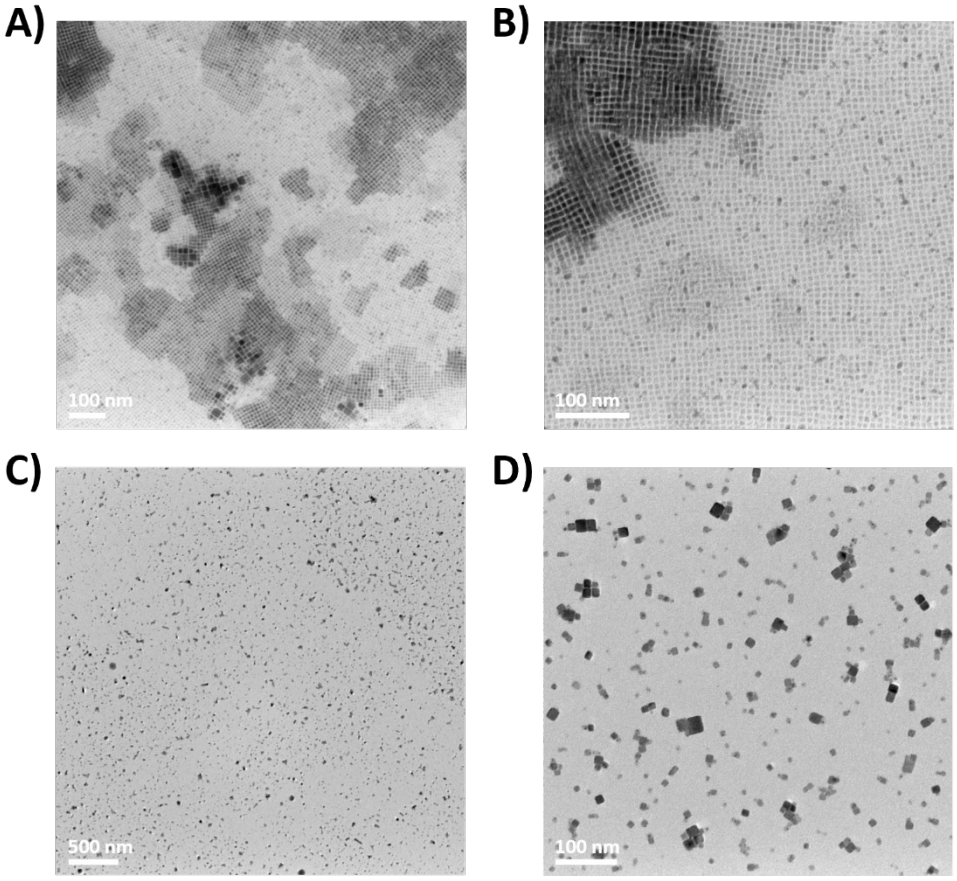

Figure S10 | Comparison of $CsPbBr_3$ QDs following dilution. TEM images of $CsPbBr_3$ QDs measured when, **A,B)** the sample is saturated in solution (21X dilution factor) and **C,D)** the sample is optically dilute in a 1 cm x 1 cm cuvette as per the standard protocol. The saturated sample was obtained by introducing a sufficiently small volume of hexanes to the pellet following centrifugation, such that the pellet cannot be fully resuspended.

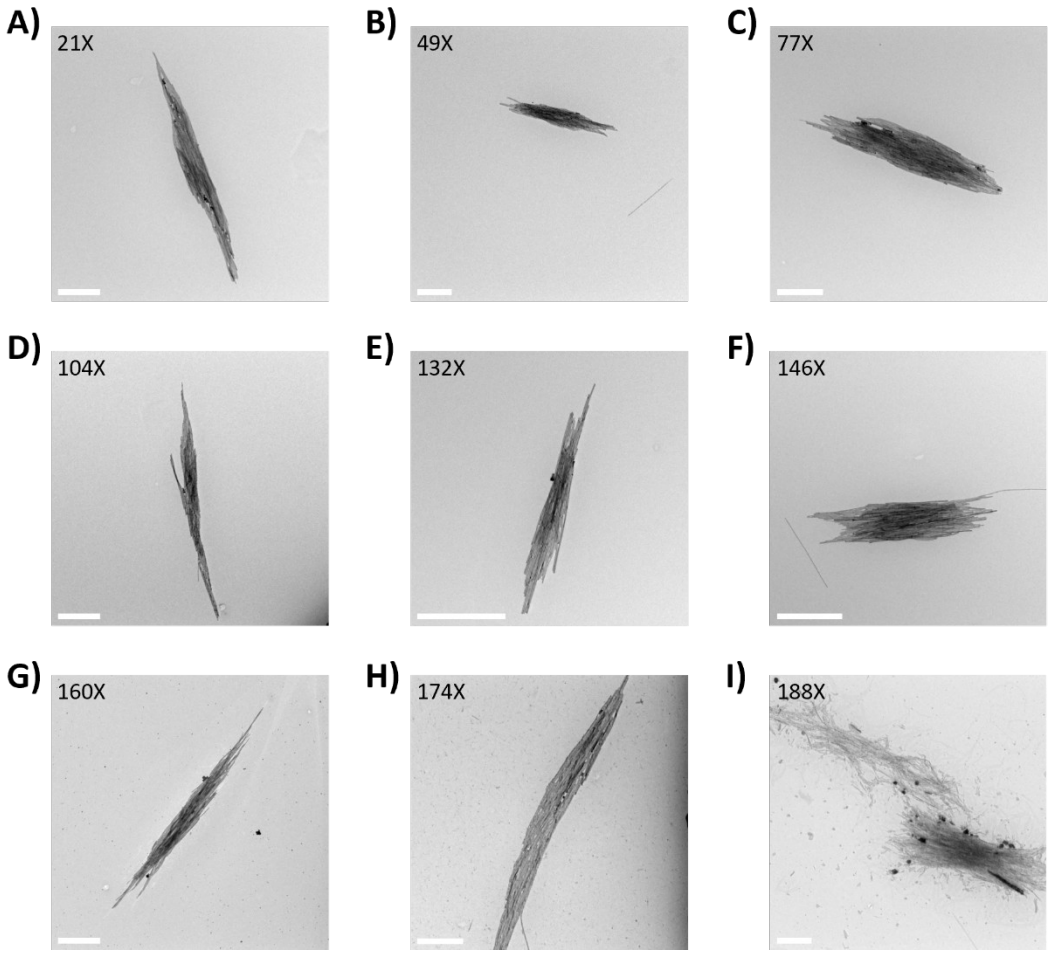

Figure S11 | TEM images of $CsPbBr_3$ NWs as a function of dilution. Scale bar: 1 μm. The dilution factors correspond to the samples measured in Figures 2-4 in the main text.

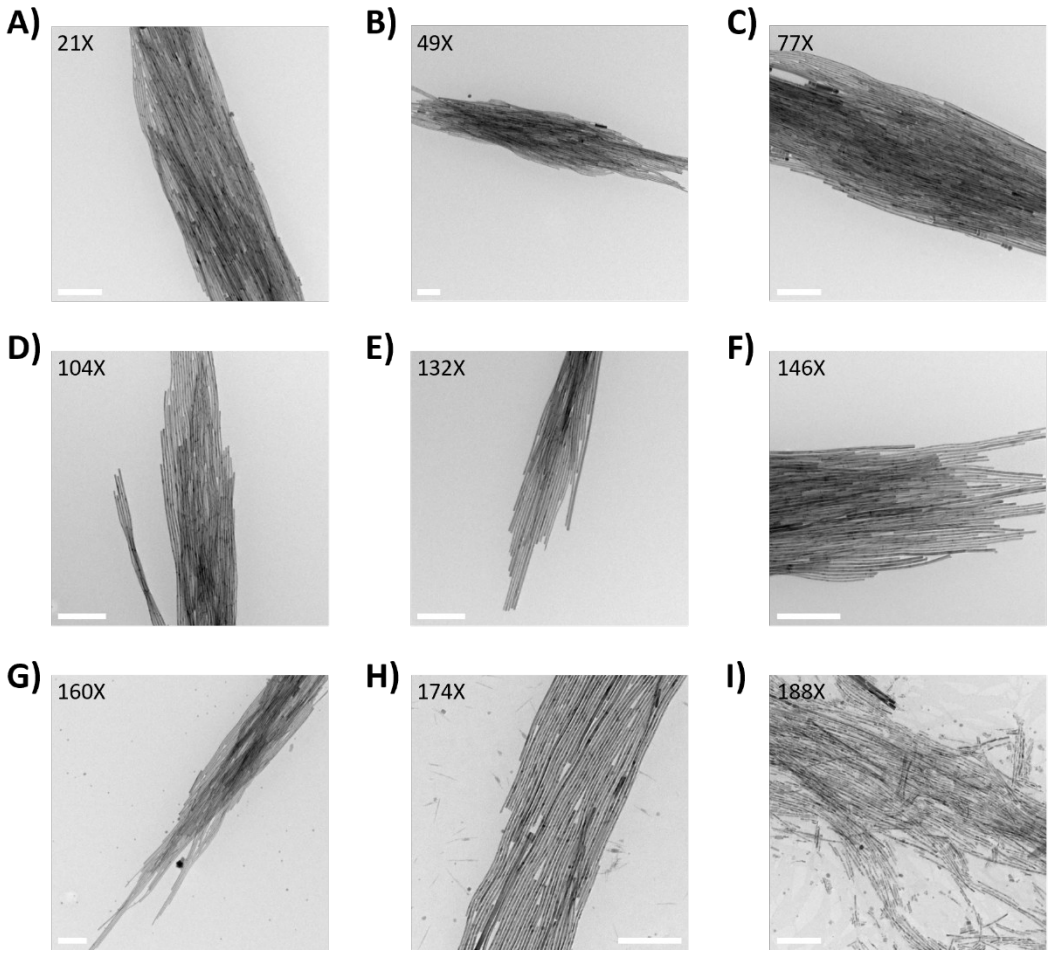

Figure S12 | TEM images of $CsPbBr_3$ NWs as a function of dilution. Scale bar: 250 nm. The dilution factors correspond to the samples measured in Figures 2-4 in the main text. This figure is just a zoomed in version of Figure S11.

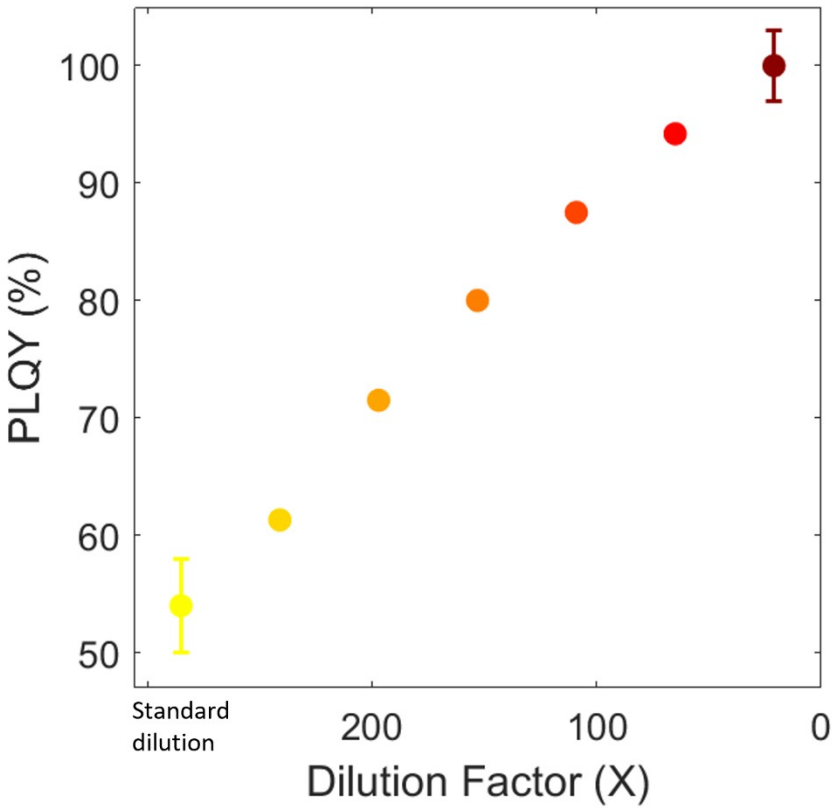

Figure S13 | The effect of dilution on the PLQY of $CsPbBr_3$ QDs.

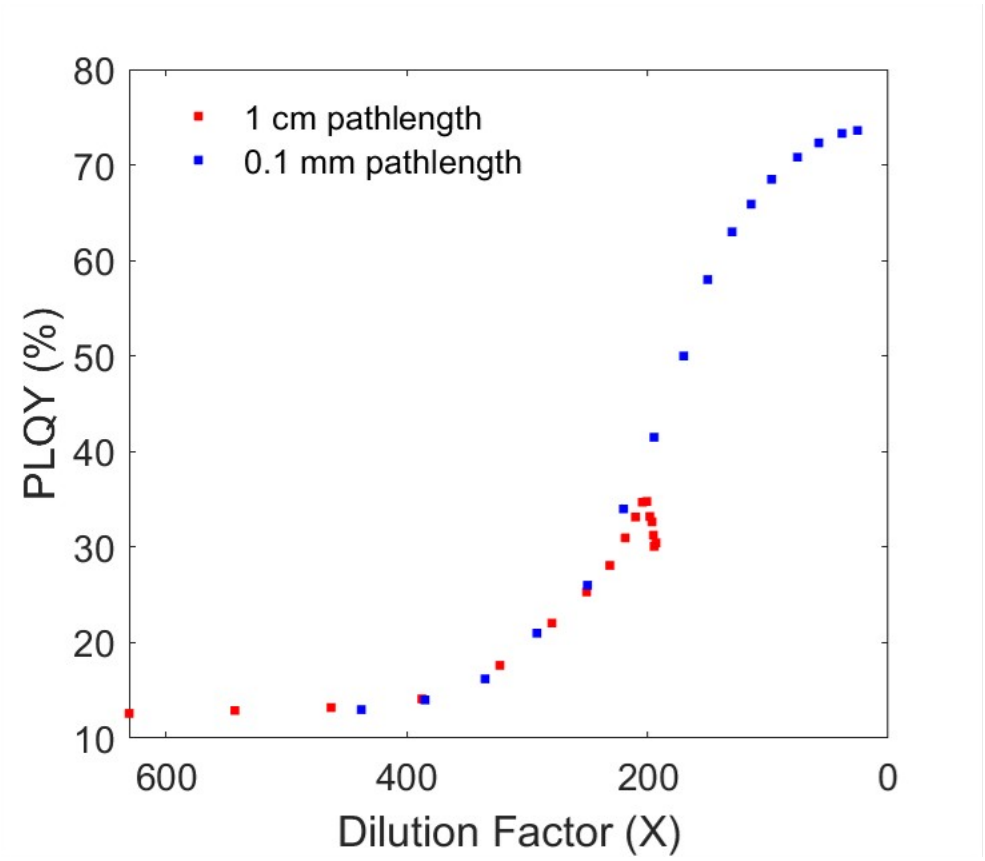

Figure S14 | Effect of dilution on the PLQY of $CsPbBr_3$ NWs in the 0.1 mm cuvette as compared to the standard 1 cm cuvette.

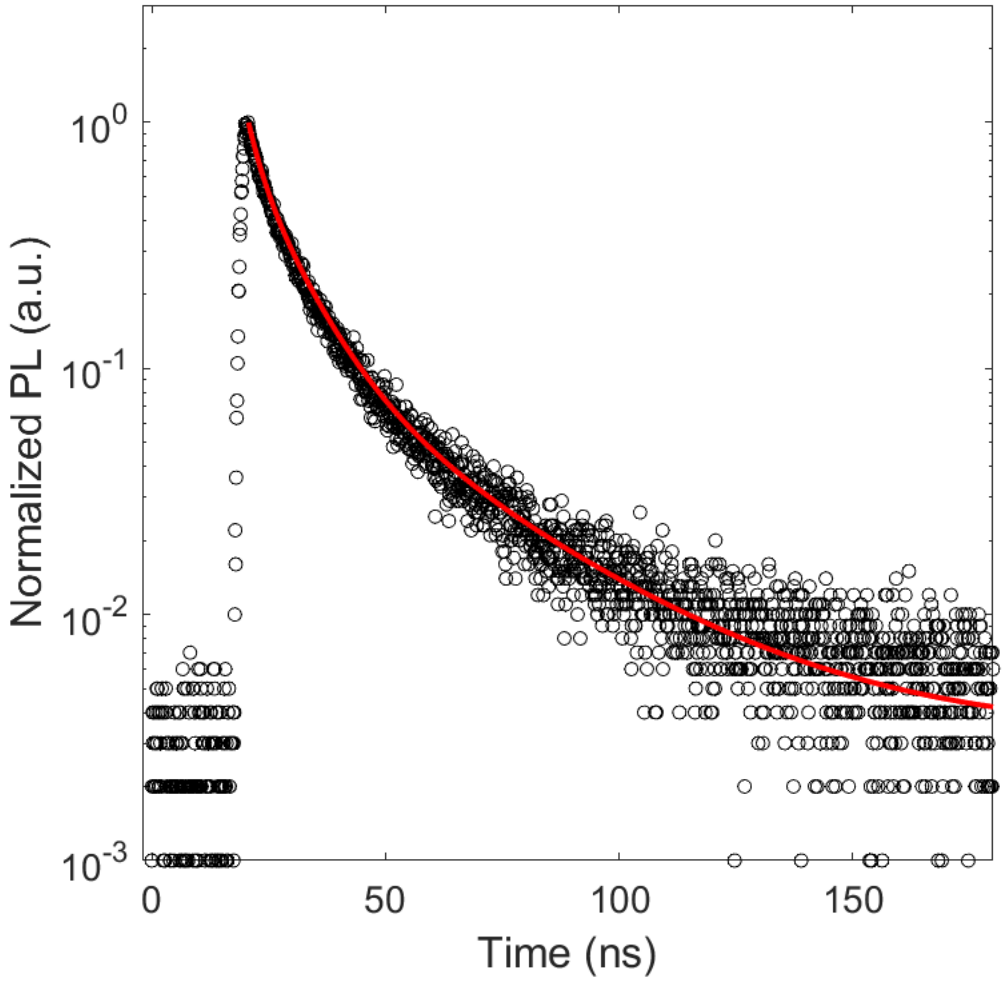

Figure S15 | The PL decay of $CsPbBr_3$ QDs measured under the standard protocol, optically dilute in a 1 x 1 cm cuvette. The PL lifetimes were τ_1=2.3 ns, τ_2=9.9 ns, and τ_3=52.9 ns, and the relative contributions were 18.4%, 78.1%, and 3.5%, respectively. The fitting error parameter was R^2=0.9949.

Dilution (X)	τ_1 (ns)	τ_2 (ns)	τ_3 (ns)	τ_{ave} (%)	B_1	B_2	B_3	Cont. 1 (%)	Cont. 2 (%)	Cont. 3 (%)	χ^2
21	7.2 ± 0.2	63 ± 2	570 ± 10	400 ± 10	693	170	58.5	10.3	21.8	67.9	1.1445
35	8.4 ± 0.3	68 ± 2	570 ± 20	400 ± 20	600	145	53.6	11.1	21.7	67.2	1.1163
49	8.1 ± 0.3	70 ± 3	590 ± 20	410 ± 20	606	134	44.9	12.0	22.7	65.3	1.1236
63	8.6 ± 0.3	66 ± 2	570 ± 20	380 ± 20	494	155	47.1	12.1	24.3	63.6	1.1283
77	7.9 ± 0.2	63 ± 2	580 ± 20	370 ± 20	613	137	36.4	14.1	24.9	61.0	1.1544
90	7.6 ± 0.2	59 ± 2	550 ± 20	340 ± 20	600	134	31.8	15.3	26.4	58.3	1.1284
104	7.6 ± 0.3	53 ± 2	420 ± 10	250 ± 10	571	139	33.2	16.8	28.8	54.4	1.1765
118	7.0 ± 0.2	55 ± 2	420 ± 10	240 ± 10	718	140	33.1	18.8	28.8	52.4	1.1530
132	6.8 ± 0.2	50 ± 2	331 ± 8	185 ± 6	644	149	36.6	18.2	31.1	50.8	1.0856
146	6.2 ± 0.2	45 ± 2	301 ± 7	159 ± 6	656	172	35.1	18.2	34.6	47.2	1.0179

Table S1 | Table of PL lifetime fitting parameters for $CsPbBr_3$ NWs as a function of dilution.

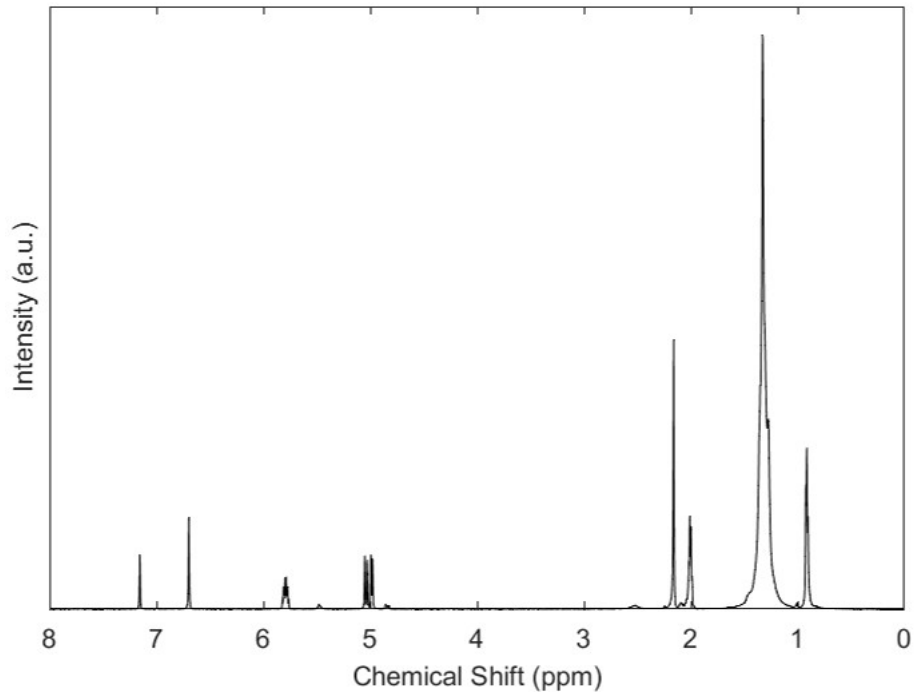

Figure S16 | The NMR spectrum of $CsPbBr_3$ NWs taken at the dilution factor of 21X.

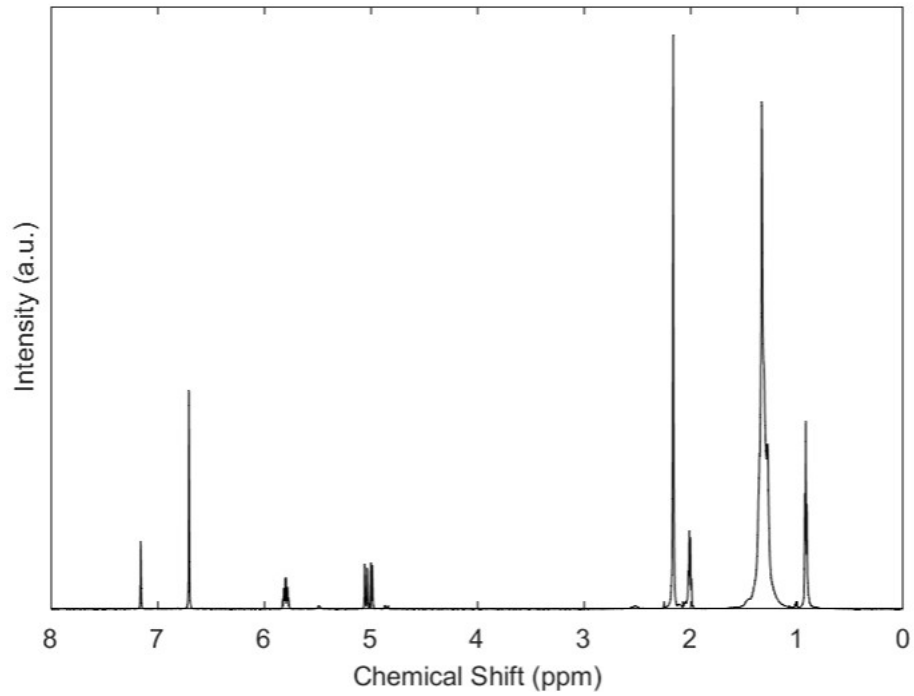

Figure S17 | The NMR spectrum of $CsPbBr_3$ NWs taken at the dilution factor of 35X.

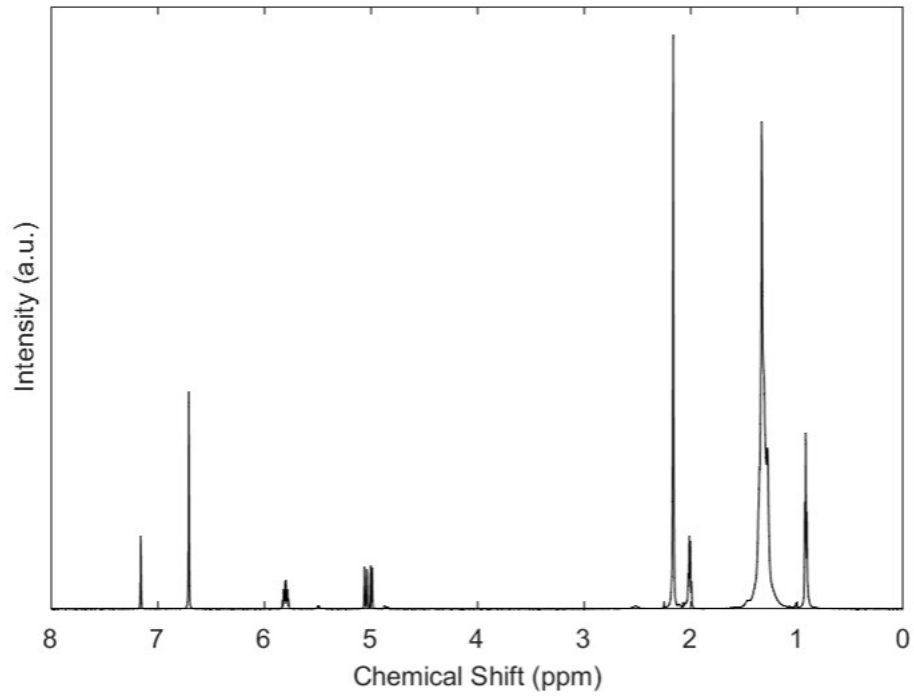

Figure S18 | The NMR spectrum of $CsPbBr_3$ NWs taken at the dilution factor of 49X.

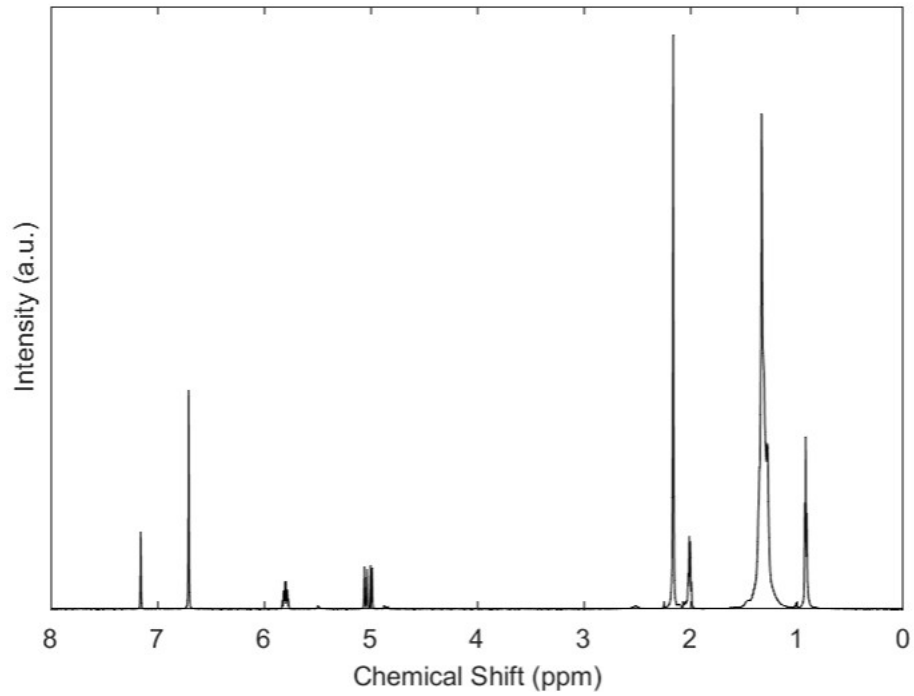

Figure S19 | The NMR spectrum of $CsPbBr_3$ NWs taken at the dilution factor of 63X.

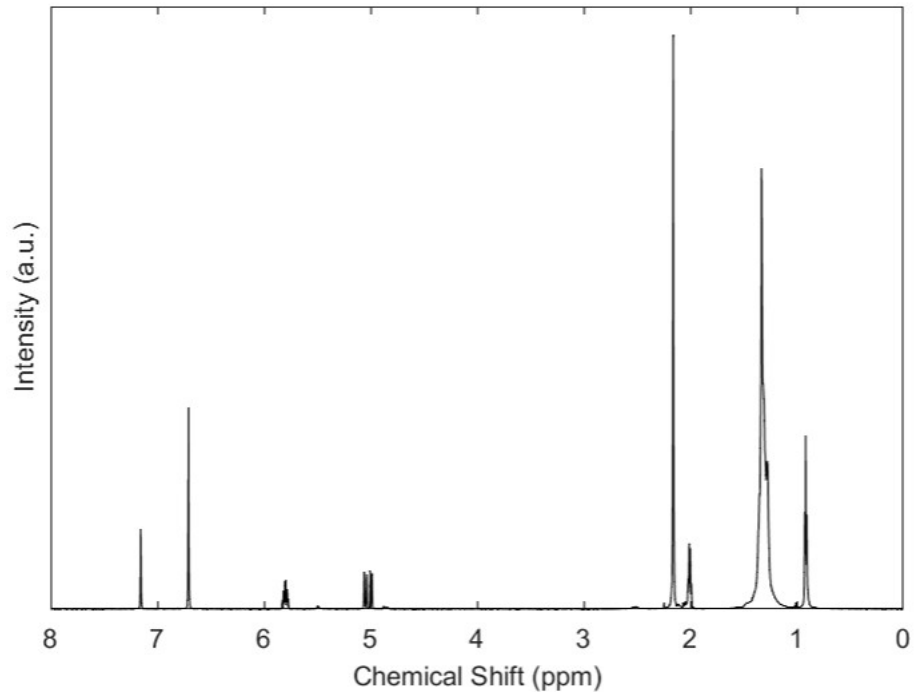

Figure S20 | The NMR spectrum of $CsPbBr_3$ NWs taken at the dilution factor of 77X.

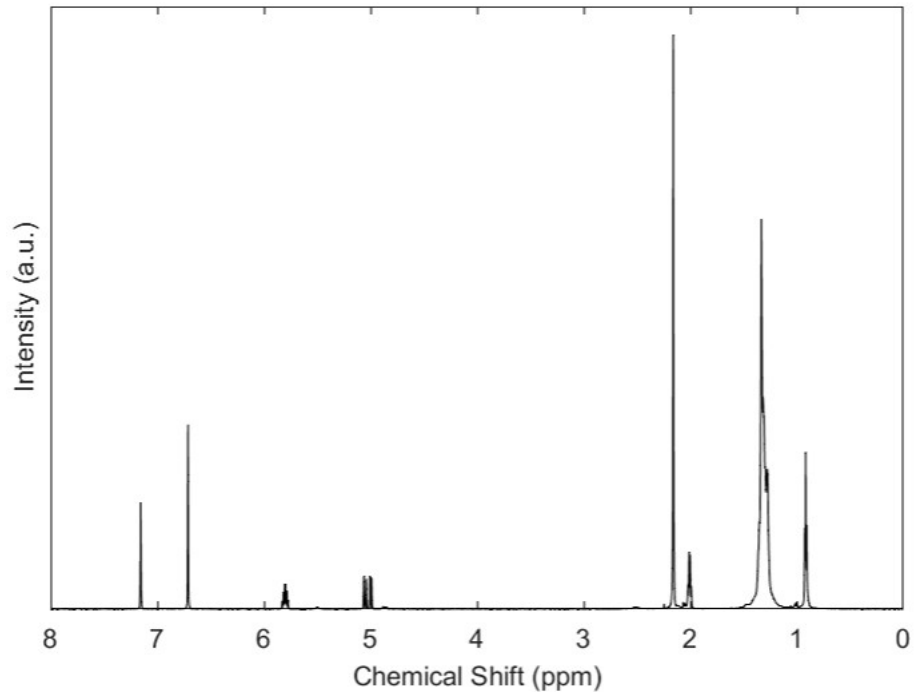

Figure S21 | The NMR spectrum of $CsPbBr_3$ NWss taken at the dilution factor of 90X.

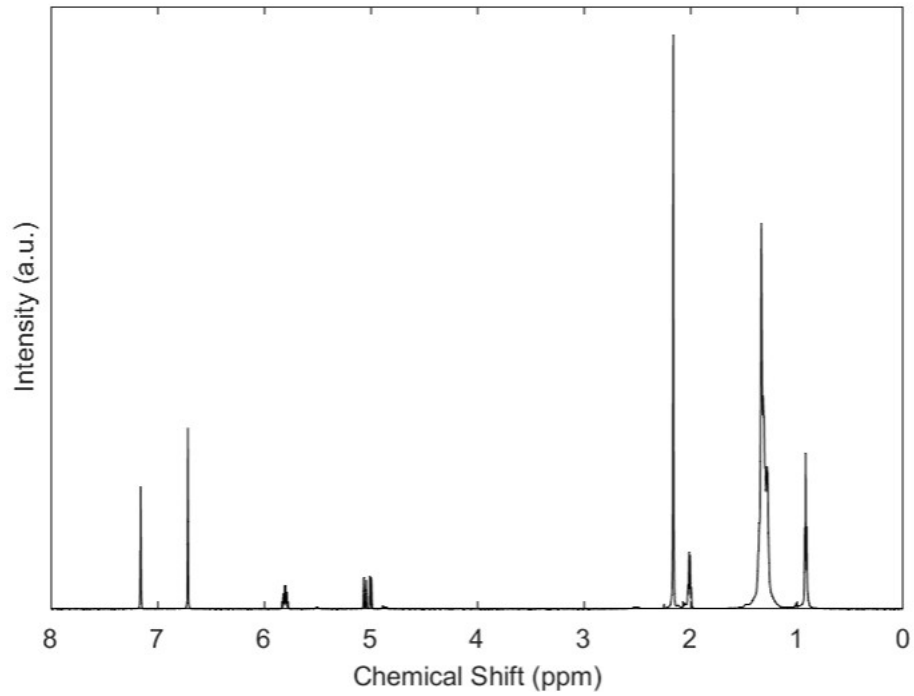

Figure S22 | The NMR spectrum of $CsPbBr_3$ NWs taken at the dilution factor of 104X.

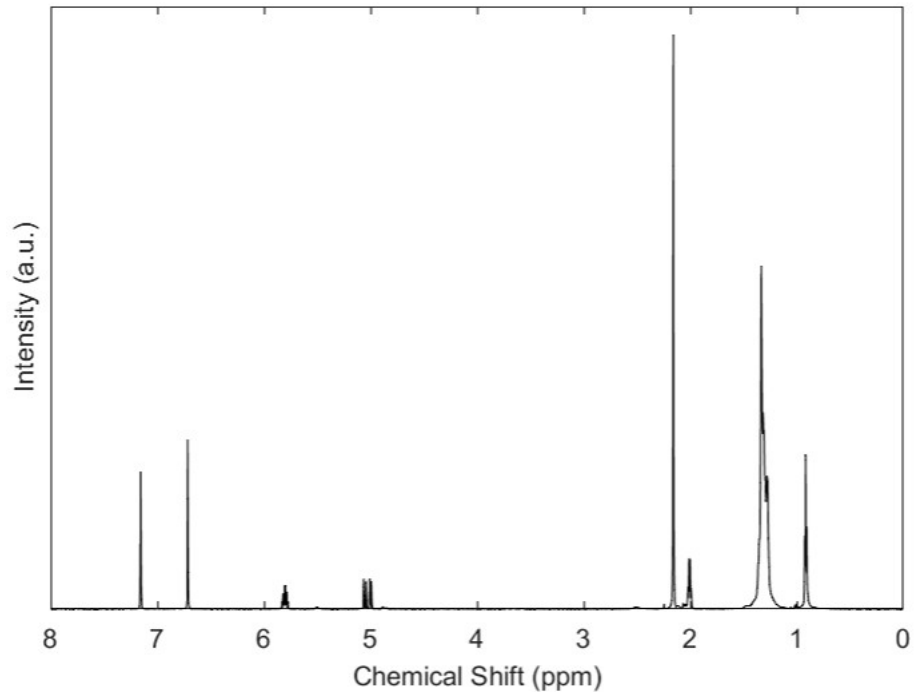

Figure S23 | The NMR spectrum of $CsPbBr_3$ NWs taken at the dilution factor of 118X.

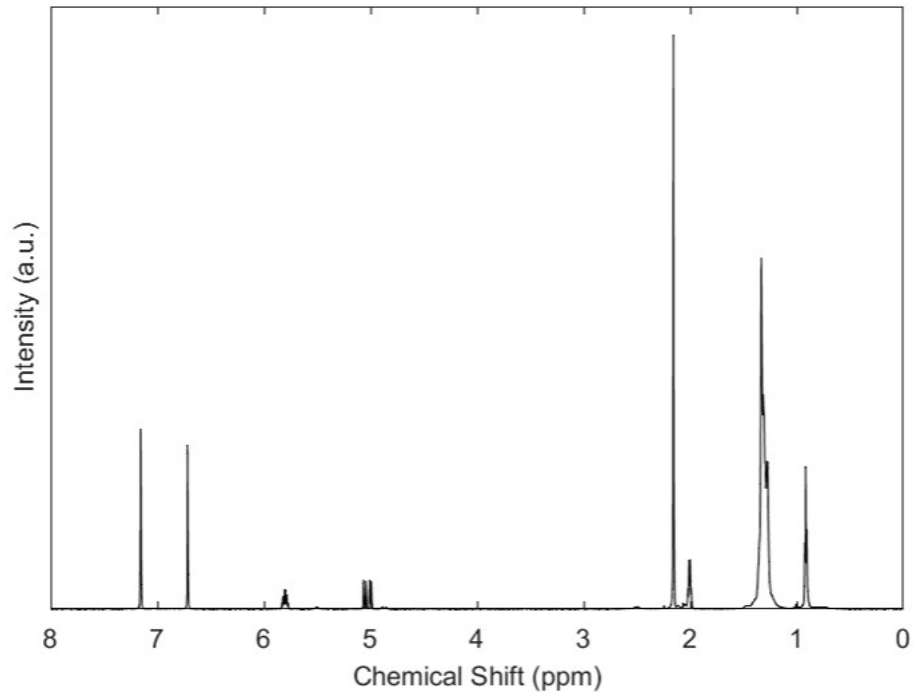

Figure S24 | The NMR spectrum of $CsPbBr_3$ NWs taken at the dilution factor of 132X.

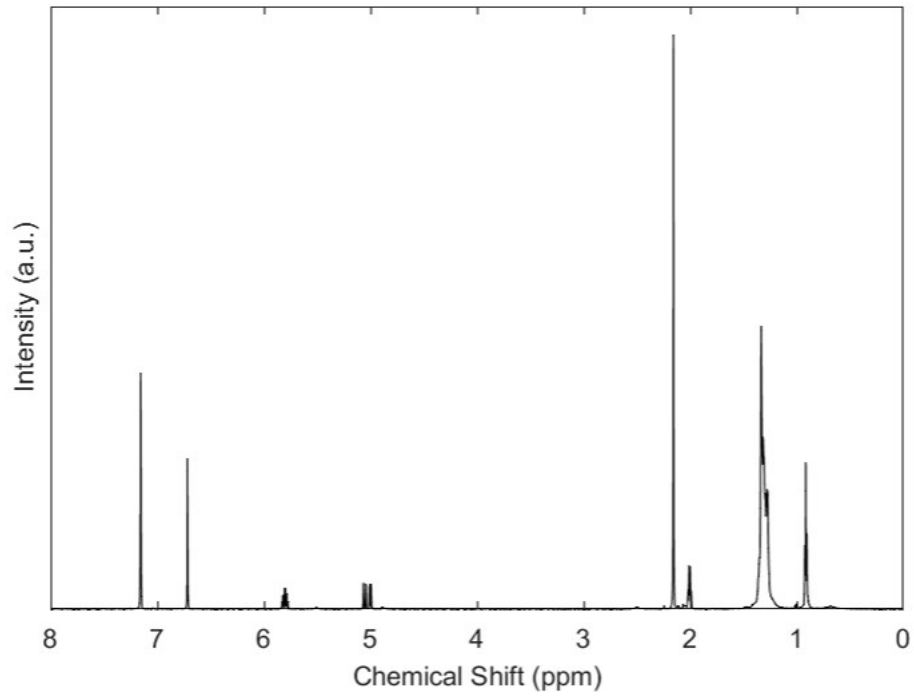

Figure S25 | The NMR spectrum of $CsPbBr_3$ NWs taken at the dilution factor of 146X.

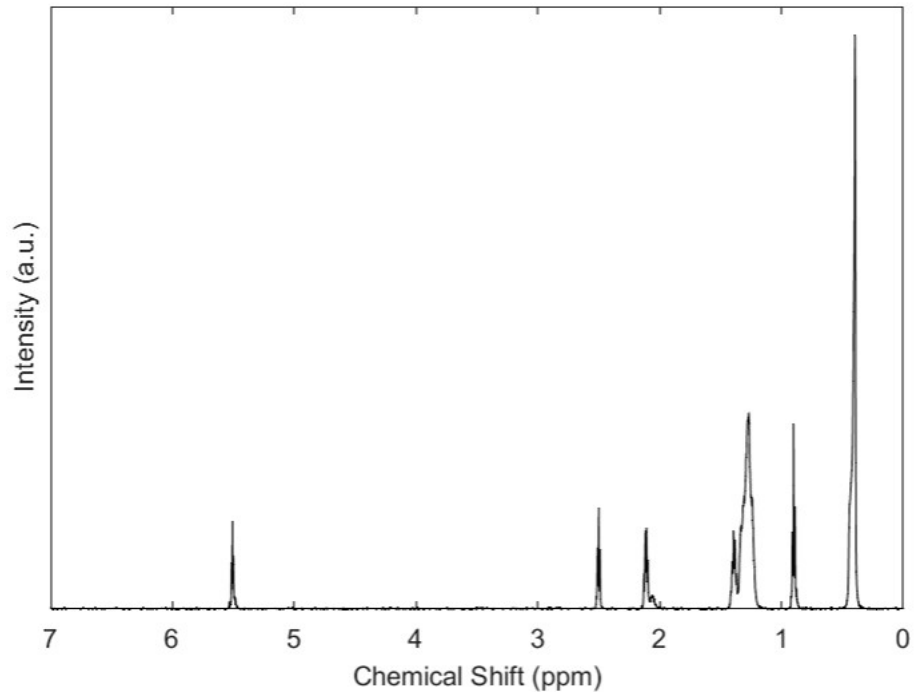

Figure S26 | The NMR spectrum of oleylamine.

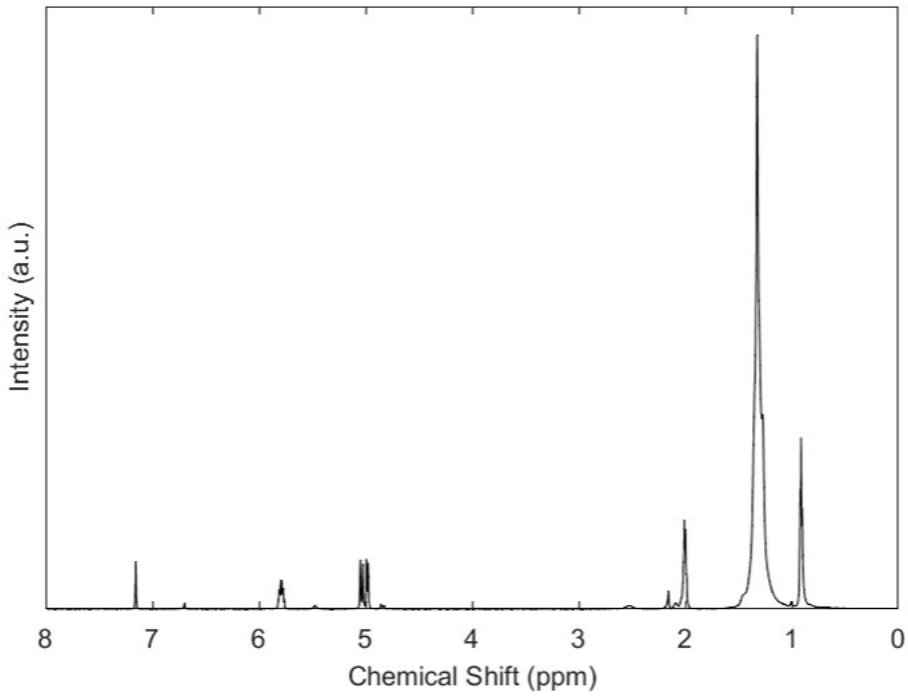

Figure S27 | The NMR spectrum of $CsPbBr_3$ QDs taken at the dilution factor of 21X.

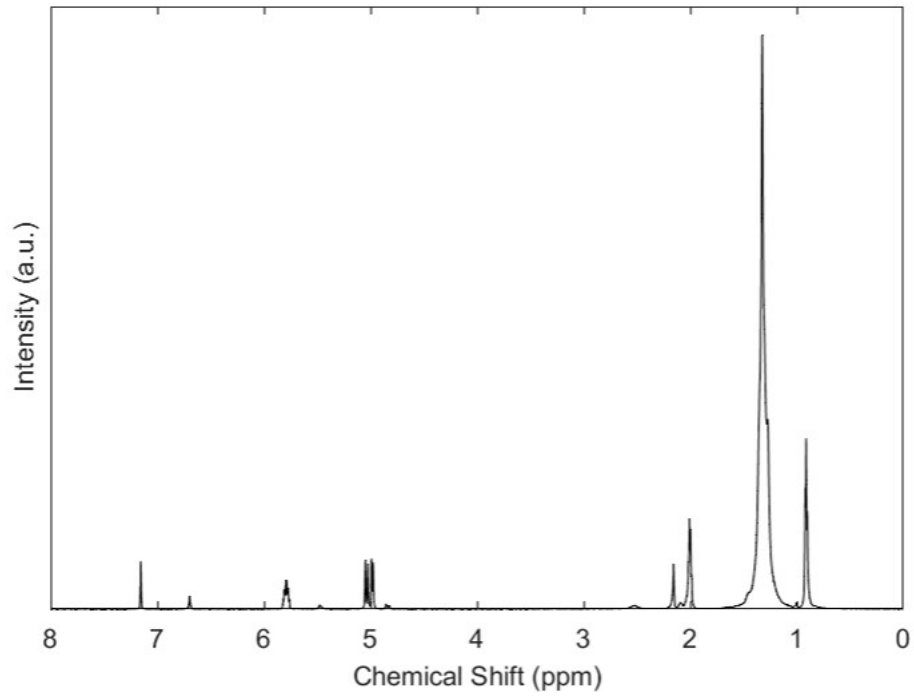

Figure S28 | The NMR spectrum of $CsPbBr_3$ QDs taken at the dilution factor of 65X.

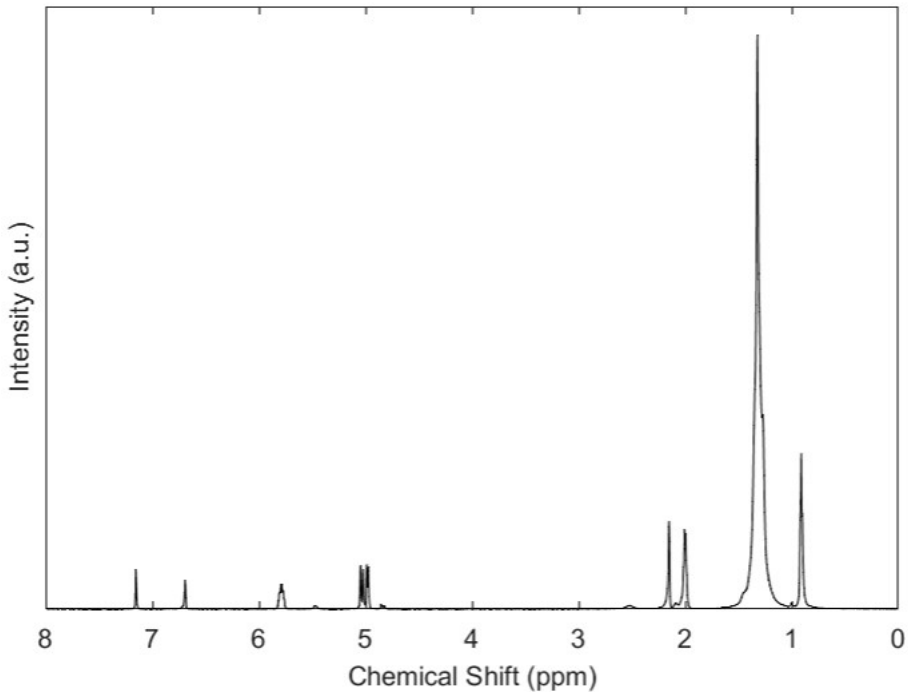

Figure S29 | The NMR spectrum of $CsPbBr_3$ QDs taken at the dilution factor of 109X.

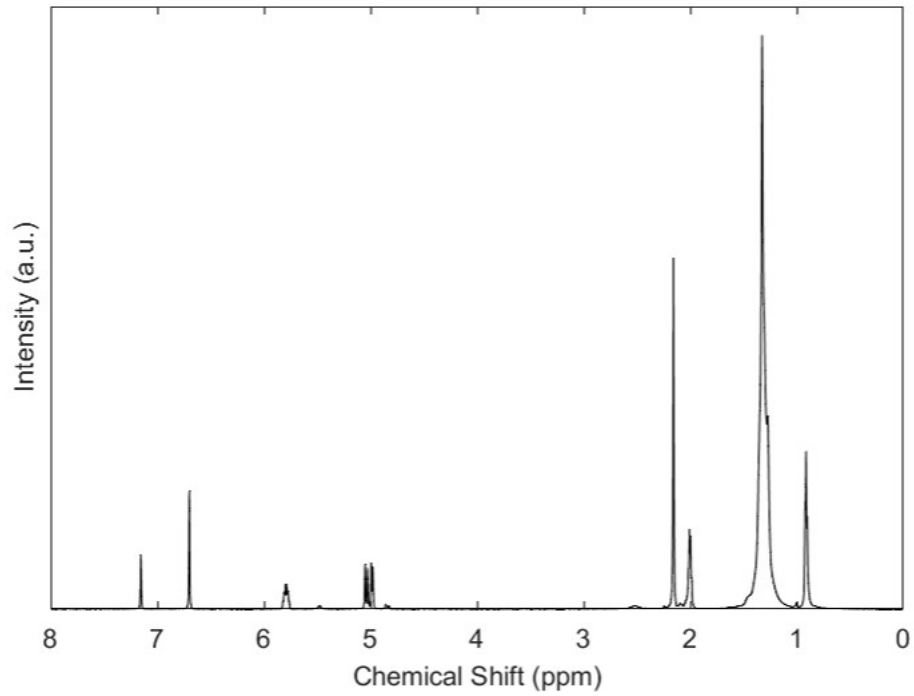

Figure S30 | The NMR spectrum of $CsPbBr_3$ QDs taken at the dilution factor of 153X.

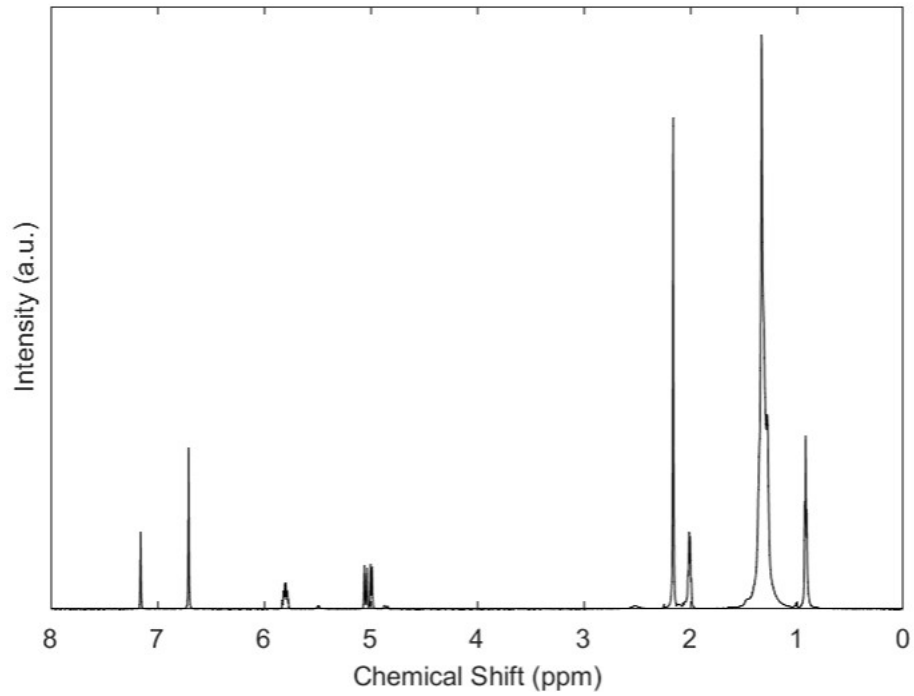

Figure S31 | The NMR spectrum of $CsPbBr_3$ QDs taken at the dilution factor of 197X.

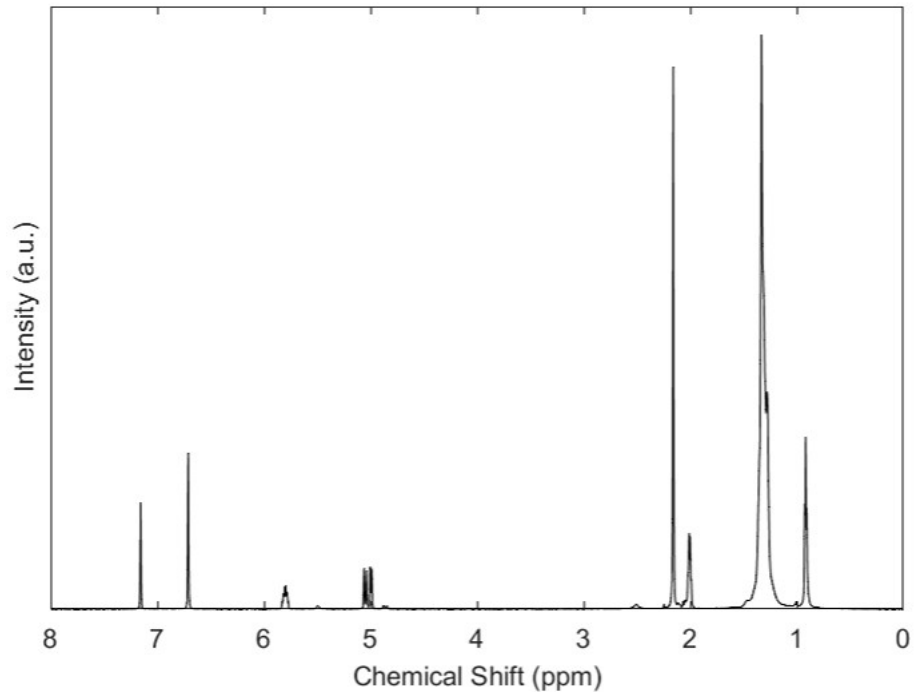

Figure S32 | The NMR spectrum of $CsPbBr_3$ QDs taken at the dilution factor of 241X.

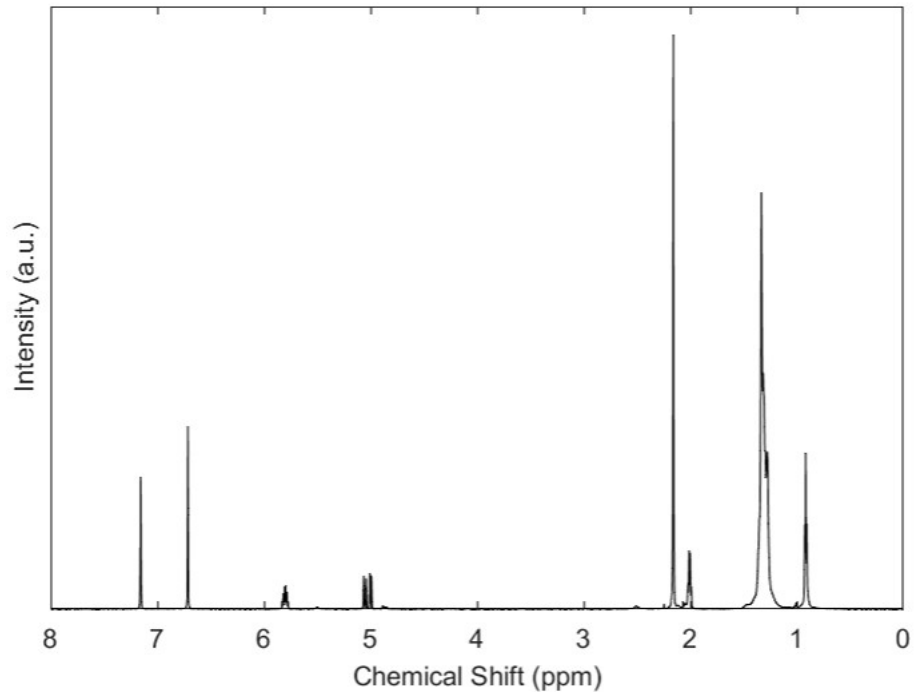

Figure S33 | The NMR spectrum of $CsPbBr_3$ QDs taken at the dilution factor of 285X.